SEISMIC CHARACTERISATION OF COAL INTERBED MULTIPLES IN COOPER BASIN, AUSTRALIA

A Thesis

Presented to

the Faculty of the Department of Earth and Atmospheric Sciences

University of Houston

In Partial Fulfillment

of the Requirements for the Degree

Master of Science

By

Chen Qi

May, 2013

SEISMIC CHARACTERISATION OF COAL INTERBED MULTIPLES IN COOPER BASIN, AUSTRALIA

Chen Qi

APPROVED:

Dr. Robert Stewart, Chairman

Dr. Fred Hilterman, Advisor

Dr. Evgeny Chesnokov

Dr. Lee Bell
Geokinetic Inc.

Dean
College of Natural Sciences and Mathematics

Acknowledgements

I am especially thankful to my supervisor, Dr. Fred Hilterman, for his insightful suggestions on my research, for his guidance throughout the Master's program, and for his willingness to share the wisdom of life with me. I would like to thank the rest of my thesis committee, Dr. Robert Stewart, Dr. Evgeny Chesnokov, and Dr. Lee Bell, for their encouragement and invaluable input to my work. I thank my friends, who are always willing to help and discuss the tough questions I encounter. Last but not the least; I thank my family for supporting me and believing in me as always.

SEISMIC CHARACTERISATION OF COAL INTERBED MULTIPLES IN COOPER BASIN, AUSTRALIA

An Abstract of a Thesis
Presented to
the Faculty of the Department of Earth and Atmospheric Sciences
University of Houston

In Partial Fulfillment
of the Requirements for the Degree
Master of Science

By
Chen Qi
May, 2013

Abstract

Apparent attenuation resulting from interbed multiples is conveniently expressed by Margraves nonstationary convolution model. A few examples of nonstationary processes are time migration, normal-moveout corrections, and forward and inverse Q filtering. Any nonstationary but linear effect can be included in the nonstationary model by an appropriate modification to the convolutional matrix. By embedding pure propagating wavelets at each earth interface in the convolutional matrix, nonstationary convolution replicates the effects of interbed multiples in the output matrix. These propagating wavelets in highly cyclic sequences, such as coal beds, include significant time delays of the primary energy, high-frequency transmission loss and a decrease of seismic resolution for primary energy contaminated with interbed multiples.

Because each column vector in the convolution matrix is associated with a primary-only reflection coefficient, the aligned convolution matrix is better defined as a wavelet dictionary. A major goal in data processing is to convert the various time series in the wavelet dictionary into short propagating wavelets that are not time varying. To assist in this task, the wavelet dictionary time series were approximated with minimum-phase equivalent Gaussian pulses.

As a measure of success, nonstationary convolution with the wavelet dictionary provided a much better synthetic match to field data than the conventional synthetic seismogram and it duplicated the results of the exact all internal multiple algorithm. By studying the computed wavelet dictionary, a time delay of $\boldsymbol{25.6ms/1000ft}$ ($\boldsymbol{305m}$) and energy loss of $\boldsymbol{74.1dB\ loss/1000ft}$ ($\boldsymbol{305m}$) for primary energy were observed beneath the coal beds. The two parameters needed to estimate the Gaussian

function from the wavelet dictionary amplitude spectra offer insight for designing future data processing algorithms to correct for the coal bed effects. However, the assumption of minimum-phase spectra for the Gaussian wavelets needs further work or different wavelets are needed to approximate the wavelet dictionary.

Contents

List of Figures

Chapter 1

Introduction

1.1 Prior research on interbed multiples

Multiple reflections have been considered noise from the beginning of seismic exploration and multiple suppression methods are often needed to observe primary events. There are several methods to process long-path multiples: horizontal stacking, f-k processing, super-long source arrays, and feedback loops. (Sengbush, 1983) However, when facing interbed multiples with strong energy in highly cyclically stratified areas, the above-mentioned methods fail to perform well.

Interbed multiples or peg-leg multiples, involve successive reflections at different interfaces so that its travel-path is not symmetric. It usually refers to short-path multiples within thin beds, which result in transferring energy from the front of a wavetrain and adding it back later, and thus is a mechanism for changing waveshape.

(Sheriff, 1991)

Numerous authors have studied interbed multiples based on 1-D stratified seismic models (normal incidence). It was first proposed by Goupillaud (1961) to compensate the effects that the near-surface stratification produces on both the character and the timing of the seismic traces. His stratified earth model has $\boldsymbol{n}$ layers defined by $\boldsymbol{n+1}$ interfaces spaced at equal traveltime intervals. This method of analysis, called communication theory, has been discussed by Robinson (1983). He proved that much of the theory of seismic wave propagation through layered medium can be expressed in the framework of communication theory.

O'Doherty and Anstey (1971) showed that the transmission process for a cyclic sequence has a high-frequency cut. They provided a formula that approximately relates the amplitude spectra of the reflection coefficient series to the amplitude spectra of the transmitted pulse. After that, Schoenberger and Levin (1974) suggested that attenuation due to layering accounted for $\mathbf{1/3}$ to $\mathbf{1/2}$ of the total attenuation observed and they suggested that interbed multiples higher than fifth order were unimportant for the two studied wells. Schoenberger and Levin (1974) verified the conclusion that interbed multiples tend to raise amplitudes at the low frequency end of the spectrum and lower those at the high frequency end.

With the advent of VSP in the $\boldsymbol{1980s}$, geophysicists measured seismic wave propagation effects much more directly and the discrepancies of the sonic log and VSP derived velocities were noticed. A credible work by Stewart et al. (1984) illustrated the time discrepancies between VSP and in-situ sonic logs. They concluded that the traveltime discrepancies between the sonic and seismic measurements are due to the multiple-induced broadening of the propagating wavelet in addition to the dispersion effect.

1.2 Nonstationary convolutional model

1.2.1 Prior work on the stationary convolutional model

The conventional, or stationary convolutional model has been used widely in seismic interpretation. According to Sheriff (1991), this model proposes that a seismic trace $\boldsymbol{f(t)}$ can be represented by the convolution of a stable wavelet $\boldsymbol{w(t)}$ with a reflectivity function $\boldsymbol{r(t)}$ plus random noise $\boldsymbol{n(t)}$

$$\boldsymbol{f(t) = w(t) * r(t) + n(t).} \tag{1.1}$$

The stationary convolutional model has the following assumptions (Yilmaz, 2001):

1. The earth is made of plane layers of constant velocity.
2. The source generates a compressional plane wave which meets layer boundaries at normal incidence which means no shear waves are generated.
3. The **propagating wavelet** is stationary. The wavelet does change shape and amplitude from the source to the receiver as it propagates within the earth.
4. The noise $\boldsymbol{n(t)}$ can be ignored.

Two kinds of wavelets, **source** and **propagating** are used in this thesis. The **source wavelet** is a stationary waveform emitted by the source and conceptually could be recorded by a receiver coincident with the source. The **propagating wavelet** refers to the wavelet that defines the shape of the seismic wavefront at any instant of time (Margrave et al., 2011).

1.2.2 Margrave's nonstationary convolutional model

A nonstationary generalization of the convolution integral is presented by Margrave (1997). The so called nonstationary convolution retains the interpretation of forming the scaled superposition of impulse responses while allowing those impulse responses to become arbitrary functions of time or position (Margrave, 1997). The stationary convolution integral is expressed as

$$\boldsymbol{f_{stat}(t) = \int_{-\infty}^{\infty} w(t-\tau)r(\tau)d\tau,} \tag{1.2}$$

where $\boldsymbol{f_{stat}}$ is the stationary seismic trace, $\boldsymbol{r}$ is the time-domain reflection coefficient series, and $\boldsymbol{w}$ is the seismic wavelet. In stationary convolution, no difference exists between the source wavelet and the propagating (seismic) wavelet. By contrast, the seismic trace expressed by nonstationary convolution for a given reflectivity function $\boldsymbol{r(t)}$ is calculated as

$$\boldsymbol{f_{nonstat}(t) = \int_{-\infty}^{\infty} w(\tau, t-\tau)r(\tau)d\tau,} \tag{1.3}$$

where $\boldsymbol{w(\tau, t-\tau)}$ has replaced the delayed wavelet $\boldsymbol{w(t-\tau)}$, thus allowing temporal evolution of the propagating wavelet (Margrave et al., 2011).

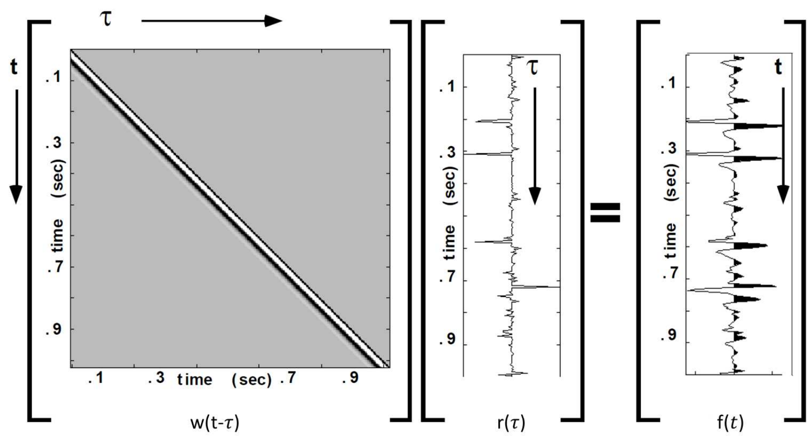

Figure 1.1: Stationary convolution as a matrix multiplication (Margrave, 1997).

1.3 Wavelet dictionary

Both stationary convolution and nonstationary convolution integrals could be recast as a matrix operation by representing $\boldsymbol{f}$ and $\boldsymbol{r}$ as column vectors and building a special "convolutional matrix" for $\boldsymbol{w}$ (Margrave, 1998) where $\boldsymbol{w}$ represents the time-varying seismic wavelet. The matrix multiplications for stationary and nonstationary convolution are illustrated in Figures 1.1 and 1.2. It is convenient to illustrate $\boldsymbol{w(u,v)}$ without the causal delay to an impulse arriving at time $\boldsymbol{u}$. The $\boldsymbol{w(u,v)}$ is named "impulse response function" by Margrave (1997) while I call it simply a "wavelet dictionary (WD)". The impulse response WD with stationary propagating wavelets and the impulse response WD with nonstationary wavelets filtered by Q are shown in Figure 1.3. These represent the wavelets that are reflected at the earth's interfaces by the primary-only reflectivity series. Any nonstationary but linear effect could be included in the nonstationary model by the appropriate modification of the convolutional matrix $\boldsymbol{w(\tau, t-\tau)}$ (Margrave, 1997). These include

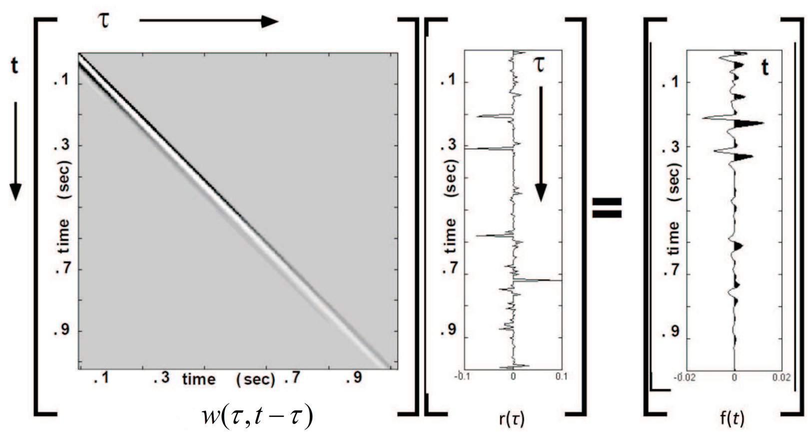

Figure 1.2: Nonstationary convolution as a matrix multiplication (Margrave, 1997).

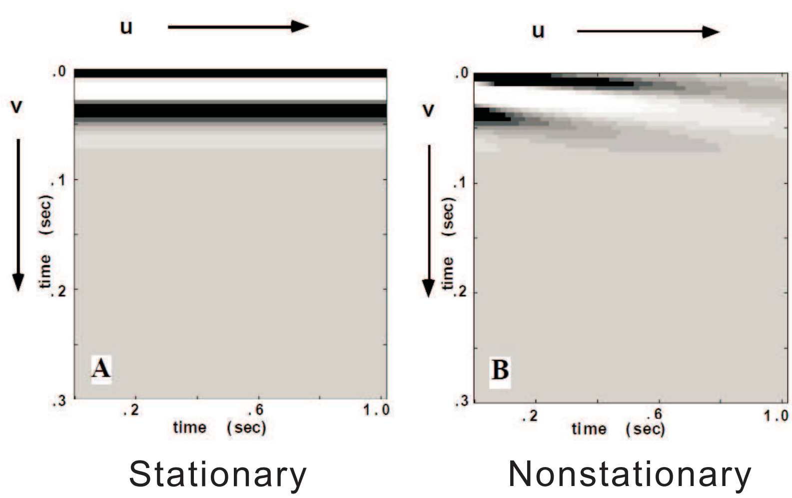

Figure 1.3: **(a)** Stationary impulse response wavelet dictionary. **(b)** Nonstationary impulse response wavelet dictionary.In the case of nonstationary, the impulse response decays in amplitude and high frequency content indicating a Q-type attenuation (Margrave, 1997).

Q attenuation, which acts like a high frequency cut filter and resembles interbed multiples,or peg-leg multiples in normal incidence (O'Doherty and Anstey, 1971; Trorey, 1962; Schoenberger and Levin, 1974). So there is no reason why interbed-multiple-induced-attenuation in normal incidence can't be embedded in the wavelet dictionary. The specific methods of doing so are illustrated in **Chapter 2**.

1.4 Thesis outline

First, the techniques for calculating a synthetic seismic trace with all related downgoing and upgoing waves at normal incidence with all internal multiples are introduced in **Chapter 2**. This method was proposed by Waters (1981). Then, the key steps to modify the WD with columns affected by interbed multiples are discussed and the algorithm to do so is shown at the end of **Chapter 2**.

Furthermore, field data are used to verify the methods discussed at the beginning of **Chapter 3**. The computed synthetic trace and wavelet dictionary proved to be powerful tools for quantitatively studying attenuation effects caused by interbed multiples. This is shown in the middle of **Chapter 3**.

At the end of **Chapter3**, the wavelet dictionary time series are approximated with mathematically-defined truncated minimum-phase equivalent Gaussian pulses.

Chapter 2

Theory and method

2.1 Synthetic seismic trace with all internal multiples

This section discusses methods for building synthetic with primary plus all internal multiples base on the methods proposed by Waters (1981).

2.1.1 Earth model description

The earth is considered as a stack of isotropic and homogenous horizontal layers whose vertical traveltime is constant. Source and receiver are located at the same position which is just below the air-earth surface. With normal incidence, only P-wave energy will be generated. Figure 2.1 illustrates the earth model and notations

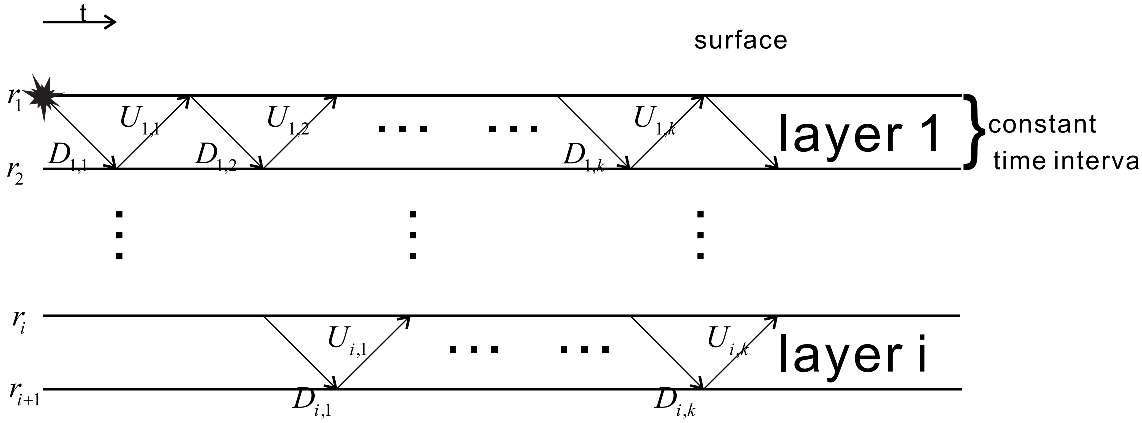

Figure 2.1: Illustration of the earth model and notations used in the thesis.

used in the thesis. For the $\boldsymbol{i'th}$ interface, $\boldsymbol{D_i}$ represents the downgoing wave that just passes the interface, $\boldsymbol{U_i}$ represents the upgoing wave that is just on the point of crossing the interface and $\boldsymbol{r_i}$ represents the reflection coefficient of the interface. The reflection coefficients in the model are defined as

$$\boldsymbol{R = (Z_2 - Z_1)/(Z_2 + Z_1) = (v_2\rho_2 - v_1\rho_1)/(v_2\rho_2 + v_1\rho_1),} \tag{2.1}$$

$$\boldsymbol{T = 1 - R,} \tag{2.2}$$

where $\boldsymbol{R}$ is reflection coefficient, $\boldsymbol{T}$ is transmission coefficient, $\boldsymbol{Z}$ is acoustic impedance, $\boldsymbol{v}$ is velocity and $\boldsymbol{\rho}$ is density. Subscript $\mathbf{1}$ means the incident medium and subscript $\mathbf{2}$ means the transmitted medium.

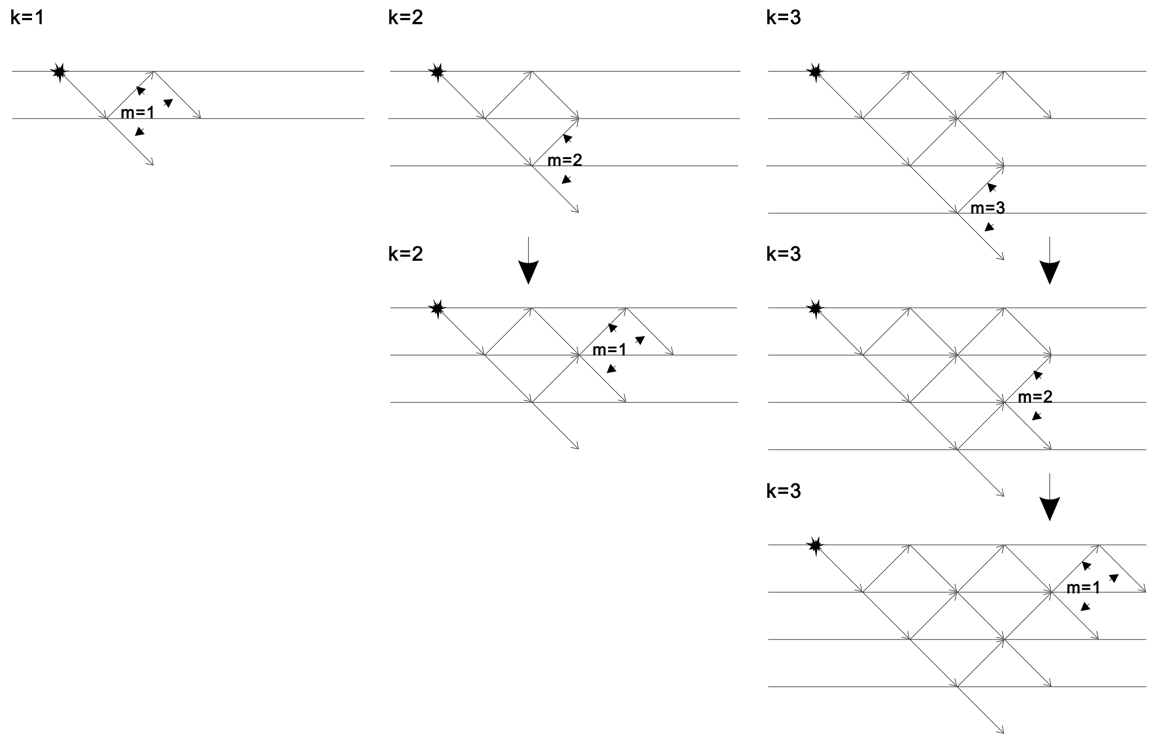

Figure 2.2: Diagram showing steps for applying the algorithm proposed by Waters (1981).

2.1.2 Algorithm for generating synthetics with all internal multiples

The all internal multiple algorithm operates with an earth model that has layers with constant traveltime, so a depth to time conversion is conducted since the well log curves are recorded as a function of depth. The algorithm to generate multiple synthetics is taken from Waters (1981). The algorithm contains two calculation loops that are illustrated in Figure 2.2 where **k** represents the outer loop counter that increases progressively from **1** to the number of layers and **m** represents the inner loop counter that decreases progressively from **k** to **1**.

For each layer, upgoing and downgoing waves are calculated using the following equations

$$\boldsymbol{U_i^{(j)} = r_i D_i^{(j)} + (1 + r_i) U_{i+1}^{(j-1)},} \tag{2.3}$$

$$\boldsymbol{D_{i+1}^{(j)} = (1 - r_i) D_i^{(j)} - r_i U_{i+1}^{(j-1)},} \tag{2.4}$$

where $\boldsymbol{D_i^{(j)}}$ means the amplitude of the downgoing wave in the $\boldsymbol{i'th}$ layer at time $\boldsymbol{(j-1)\Delta T}$ relative to the time the downgoing wave just enters the $\boldsymbol{i'th}$ layer and $\boldsymbol{U_i^{(j)}}$ means the amplitude of the upgoing wave in the $\boldsymbol{i'th}$ layer at time $\boldsymbol{(j+1)\Delta T}$ relative to the time the downgoing wave just enters the $\boldsymbol{i'th}$ layer. $\boldsymbol{\Delta T}$ represents the constant two-way traveltime in each layer.

After applying Waters (1981) algorithm on the earth model defined by a series of reflection coefficients, upgoing and downgoing waves in each layer are derived and the surface synthetic seismic trace is computed by

$$\boldsymbol{g = U_1 - r_1 U_1,} \tag{2.5}$$

where $\boldsymbol{g}$ represents the surface synthetic trace with primary and all internal multiple reflections, $\boldsymbol{U_1}$ represents the upgoing wave in the first layer and $\boldsymbol{r_1}$ represents the surface reflection coefficient.

2.2 WD affected by interbed multiples

This section discusses the key steps to modify WD with columns affected by interbed multiples. At the end of the section, the algorithm of generating pure propagating wavelets for each interface is given.

2.2.1 Pure isolated reflection

O'Doherty and Anstey (1971) used the term "pure isolated reflection" to define the waveshape of an impulse that transmits down and back with all interbed multiples considered. Here I define "pure isolated reflection" as the reflection from the transmitted wave alone.

Referring to Figure 2.3, imagine a large increase in acoustic impedance far beneath the layered media where it generates a large reflection coefficient at the interface $\boldsymbol{B}-\boldsymbol{B}$. The reflection from $\boldsymbol{B}-\boldsymbol{B}$ is NOT affected with interbed multiples that exist after the last reflector $\boldsymbol{A}-\boldsymbol{A}$. This reflection is called a **pure isolated reflection** from interface $\boldsymbol{B}-\boldsymbol{B}$. Notice even in the absence of Q attenuation, the first part of the transmitted downgoing wavelet is no longer a single impulse, but a low-frequency wavelet whose amplitude is largely determined by interbed multiples arriving from high acoustic impedance contrasts. This interval time $\boldsymbol{T}-\boldsymbol{W}$ was called the transmission width by Trorey (1962) and all downgoing arrivals occurring within this interval are considered to be **primary energy**. The techniques for calculating a synthetic seismic trace with all related downgoing and upgoing waves at normal incidence with all internal multiples has been given in the previous section. However, some manipulations need to be done based on the previous algorithm to calculate pure isolated reflections and are introduced in the end of this section.

2.2.2 Wavelet dictionary and pure isolated reflection

Trorey (1962) stated that the primary pulse reflected from a specific interface, as

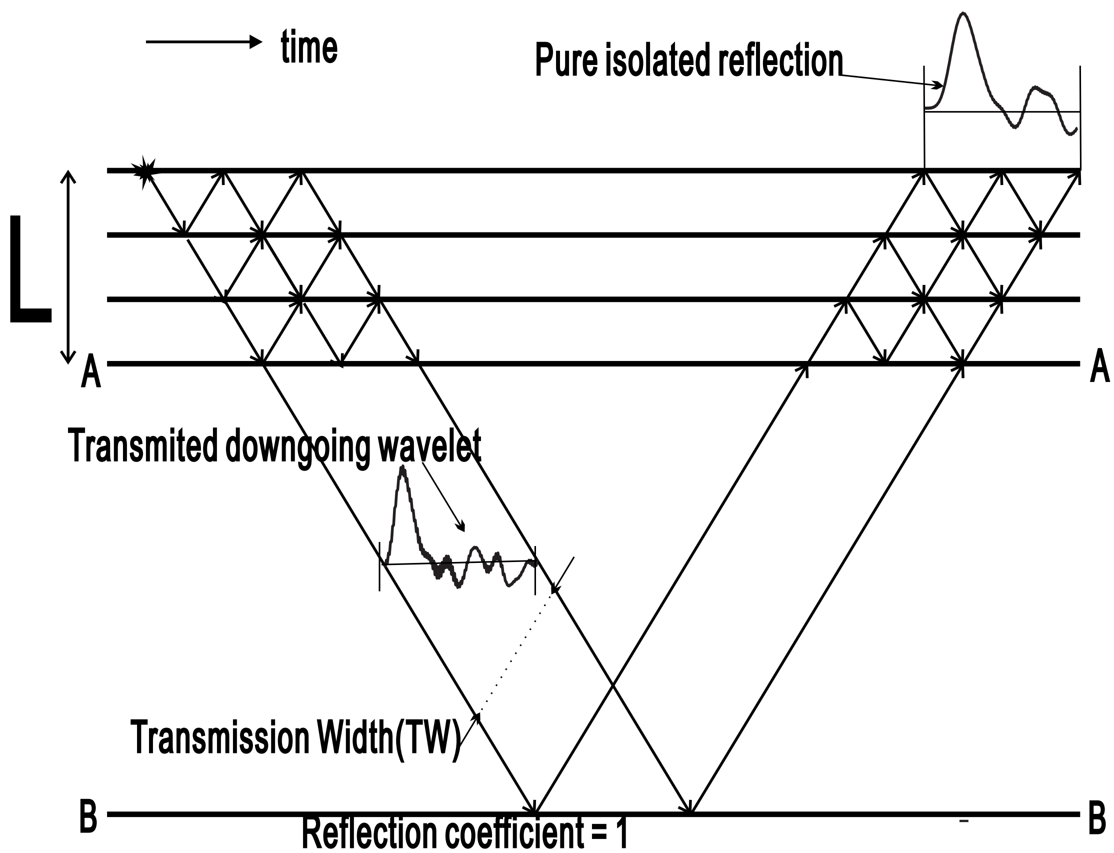

Figure 2.3: Pure isolated reflection and its transmission width.

observed at the surface, is assumed to consist of all possible reflections involving that interface within a time $\boldsymbol{T-W}$ or less after the direct arrival from the specific interface. This means the surface seismic trace is generated by linear superposing pure isolated reflections from all interfaces and the operation is recast into a matrix multiplication as

$$\begin{bmatrix} \vdots \\ \boldsymbol{f(1)} \\ \boldsymbol{f(2)} \\ \boldsymbol{f(3)} \\ \boldsymbol{f(4)} \\ \vdots \end{bmatrix} = \begin{bmatrix} \vdots & \vdots & \vdots & \vdots & \vdots \\ \vdots & \boldsymbol{l(1,1)} & \boldsymbol{0} & \boldsymbol{0} & \vdots \\ \vdots & \boldsymbol{l(1,2)} & \boldsymbol{l(2,1)} & \boldsymbol{0} & \vdots \\ \vdots & \boldsymbol{l(1,3)} & \boldsymbol{l(2,2)} & \boldsymbol{l(3,1)} & \vdots \\ \vdots & \boldsymbol{l(1,4)} & \boldsymbol{l(2,3)} & \boldsymbol{l(3,2)} & \vdots \\ \vdots & \vdots & \vdots & \vdots & \vdots \end{bmatrix} \begin{bmatrix} \vdots \\ \boldsymbol{1} \\ \boldsymbol{1} \\ \boldsymbol{1} \\ \boldsymbol{1} \\ \vdots \end{bmatrix}, \tag{2.6}$$

where $\boldsymbol{l(u,v)}$ represents the $\boldsymbol{v'th}$ sample of the pure isolated reflection from the reflector whose two-way traveltime equals to $\boldsymbol{u}$. Accordingly, the nonstationary convolution (equation 1.3) could also be expressed in matrix form as

$$\begin{bmatrix} \vdots \\ \boldsymbol{f(1)} \\ \boldsymbol{f(2)} \\ \boldsymbol{f(3)} \\ \boldsymbol{f(4)} \\ \vdots \end{bmatrix} = \begin{bmatrix} \vdots & \vdots & \vdots & \vdots & \vdots \\ \vdots & \boldsymbol{w(1,1)} & \boldsymbol{0} & \boldsymbol{0} & \vdots \\ \vdots & \boldsymbol{w(1,2)} & \boldsymbol{w(2,1)} & \boldsymbol{0} & \vdots \\ \vdots & \boldsymbol{w(1,3)} & \boldsymbol{w(2,2)} & \boldsymbol{w(3,1)} & \vdots \\ \vdots & \boldsymbol{w(1,4)} & \boldsymbol{w(2,3)} & \boldsymbol{w(3,2)} & \vdots \\ \vdots & \vdots & \vdots & \vdots & \vdots \end{bmatrix} \begin{bmatrix} \vdots \\ \boldsymbol{r(1)} \\ \boldsymbol{r(2)} \\ \boldsymbol{r(3)} \\ \boldsymbol{r(4)} \\ \vdots \end{bmatrix}, \tag{2.7}$$

where $\boldsymbol{w(u,v)}$ represents the $\boldsymbol{v'th}$ sample of the surface received wavelet with the arrival time $\boldsymbol{u}$ and $\boldsymbol{r(u)}$ represents time domain reflection coefficient associated with the arrival time $\boldsymbol{u}$.It is clear that

$$\boldsymbol{w(u,v) = l(u,v)/r(u),} \tag{2.8}$$

which means that pure propagating wavelets in WD are calculated as the pure isolated reflections divided by the corresponding reflection coefficient.

2.2.3 Algorithm for generating pure isolated reflection and pure propagating wavelet

In order to compute the pure isolated reflection from interface $\boldsymbol{k+1}$, the transmitted downgoing wavelet (refer to Figure 2.3) in layer $\boldsymbol{k}$ is computed. For computing the downgoing wavelet in layer $\boldsymbol{k}$, set the reflection coefficients below interface $\boldsymbol{k}$ to zero and compute the transmitted downgoing wavelet using the Waters (1981) algorithm. In order to calculate the surface arrival for the transmitted downgoing wavelet reflected by interface $\boldsymbol{k+1}$, a pseudo impulse source is arranged at the bottom of layer $\boldsymbol{k}$ with additional interface $\boldsymbol{k+1}$ set alive (recall that all reflection coefficients below interface $\boldsymbol{k}$ have been set to zero when calculating the transmitted downgoing wavelet).

The impulse response measured in the first layer convolved with the transmitted downgoing wavelet is the pure propagating wavelet from interface $\boldsymbol{k+1}$ (Figure 2.4). The pure isolated reflection from interface $\boldsymbol{k+1}$ equals to the corresponding pure propagating wavelet factored by $\boldsymbol{r(k+1)}$.

Since the program for calculating synthetics with all related downgoing waves

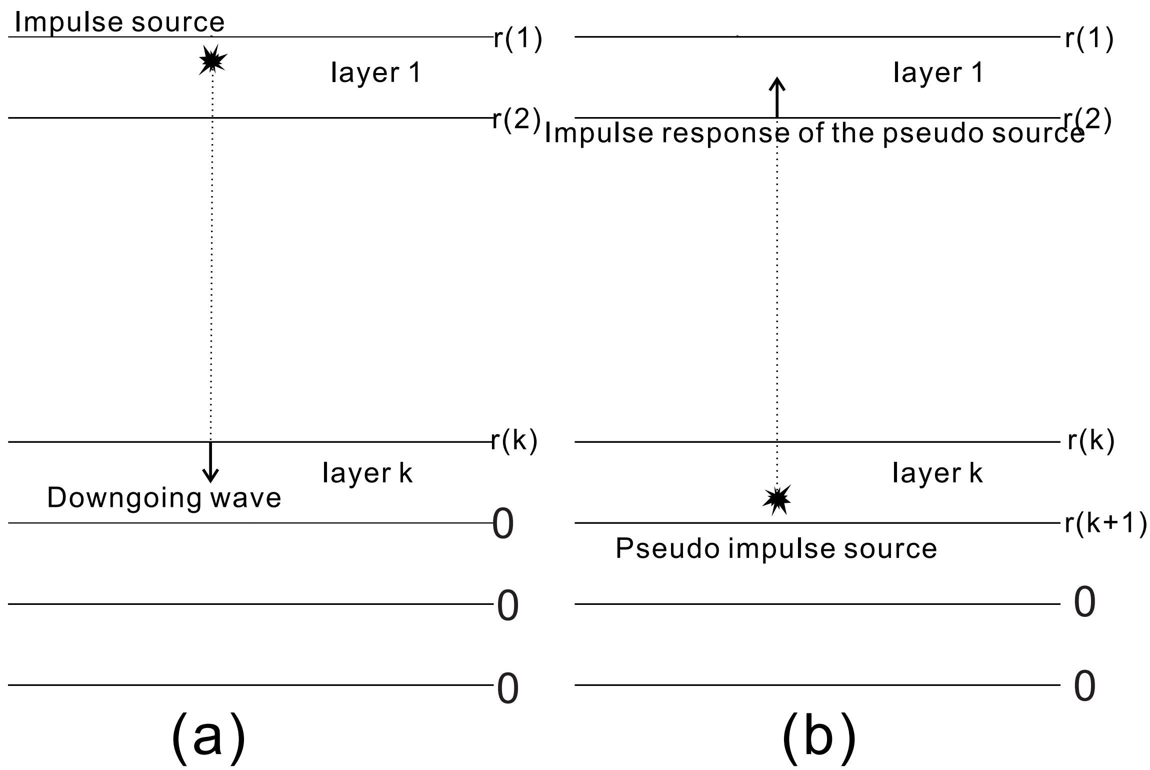

Figure 2.4: Diagram showing models used for generating the reflection wavelet whose arrival time is $(\boldsymbol{k}+\mathbf{1})\boldsymbol{\Delta T}$. **(a)** Model for computing downgoing wave and **(b)** model for computing upgoing impulse response of the pseudo source located in layer $\boldsymbol{k}$. The $(\boldsymbol{k}+\mathbf{1})'\boldsymbol{th}$ reflector is set to zero when computing the downgoing wave while it is set to alive when computing the upgoing impulse response.

has already been coded, it is time saving to use the previous code to compute the impulse response from the bottom source. The upgoing wave in the first layer excited by the bottom source is equivalent to the downgoing wave in the $\boldsymbol{k'th}$ layer excited by the surface source if the reflection coefficients used in the latter calculation are sign reversed and order flipped. See Figure 2.5(b).

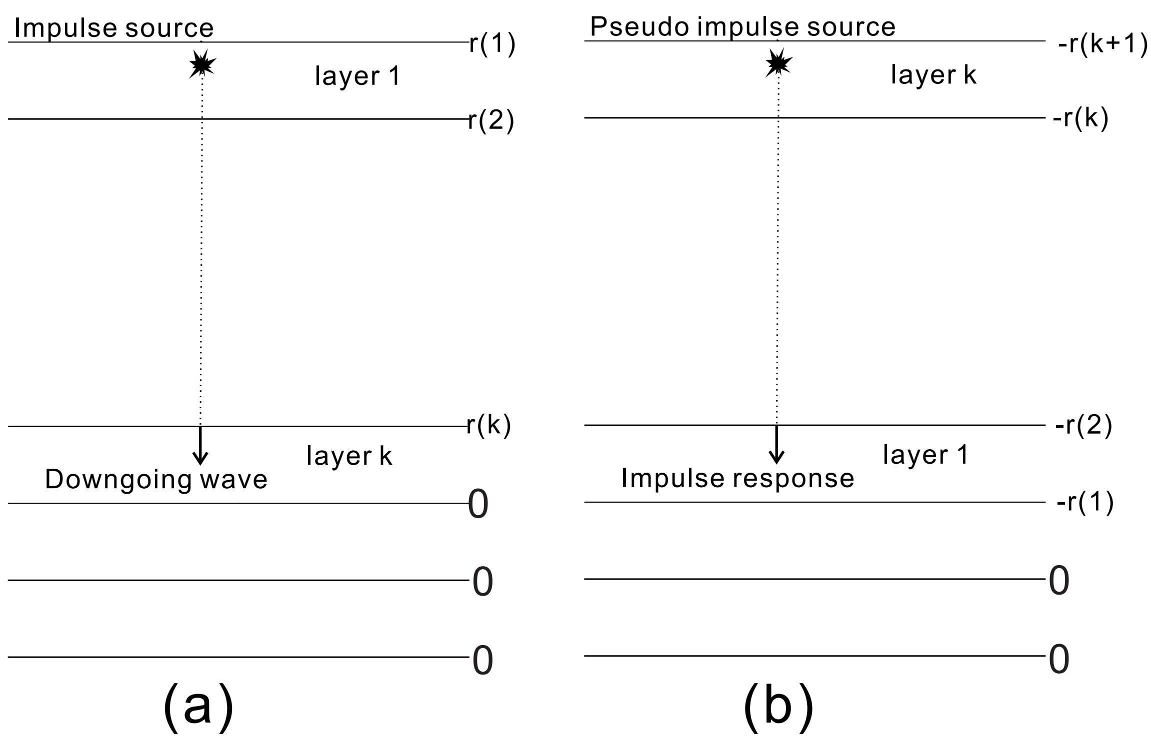

Figure 2.5: Two models that are inserted into Waters (1981) algorithm to compute the transmitted downgoing wave and the pseudo-source impulse response.

Chapter 3

Field data analysis

In this chapter, interbed multiples from field data in the Cooper Basin, Australia are analyzed and the accuracy of doing nonstationary convolution to simulate the attenuation effects caused by interbed multiples is tested.

3.1 Data introduction

Cooper Basin is a sedimentary basin which is located mainly in the northeastern part of South Australia and extends into South West Queensland. Oil and gas exploration in the basin began in **1962**. Because the oil and gas deposits in Cooper Basin tend to be fairly small and fragmentary, the resolution requirement for seismic exploration is relatively high. However, in places where coal beds dominate seismic exploration fails because the interbed multiples generated among the coal beds lower the propagating wavelets high-frequency content and delay the arrival time. Numerous exploration discoveries in the coal bed region of Cooper Basin have been associated with differential drape on top of the upper coal beds. With shale compacting more than sand, sand channels incised in the coal beds near the top of the coal formations are thicker leaving a positive time high above the channel.These drape effects are not contaminated with interbed multiples. However, new prospects in and below the coal beds are desired and this requires addressing the problem of interbed multiples.

3.1.1 Well log data

Curves from a well located in the middle of a $\boldsymbol{3D}$ seismic survey with modern processing are plotted in Figure 3.1. The density curve was logged from $\mathbf{8300}$ to $\boldsymbol{9900ft}$ ($\boldsymbol{2530-3018m}$) (MD). A pseudo-density curve was generated from $\boldsymbol{2900ft}$ ($\boldsymbol{884m}$) to $\boldsymbol{8300ft}$ ($\boldsymbol{2530m}$) using a Gardner-type transform on the velocity and lithology curves. The coal bed intervals have been enlarged and are shown in Figure 3.2. The density and velocity curves have been linearly interpolated from the surface to $\boldsymbol{2900ft}$ ($\boldsymbol{884m}$).

The sand and shale formations in the coal bed intervals have almost the same density and sonic values which are approximately $\boldsymbol{2.5g/cm^3}$ and $\boldsymbol{67\mu s/ft}$ ($\boldsymbol{220\mu s/m}$) while the coal beds have an extremely low density and sonic values of approximately $\boldsymbol{1.27g/cm^3}$ and $\boldsymbol{133\mu s/ft}$ ($\boldsymbol{436\mu s/m}$) respectively and this makes the sand/coal(shale/coal) reflection coefficient approach $\boldsymbol{-0.6}$.

The coal layer thickness statistics are shown in Figure 3.3. The number of coal

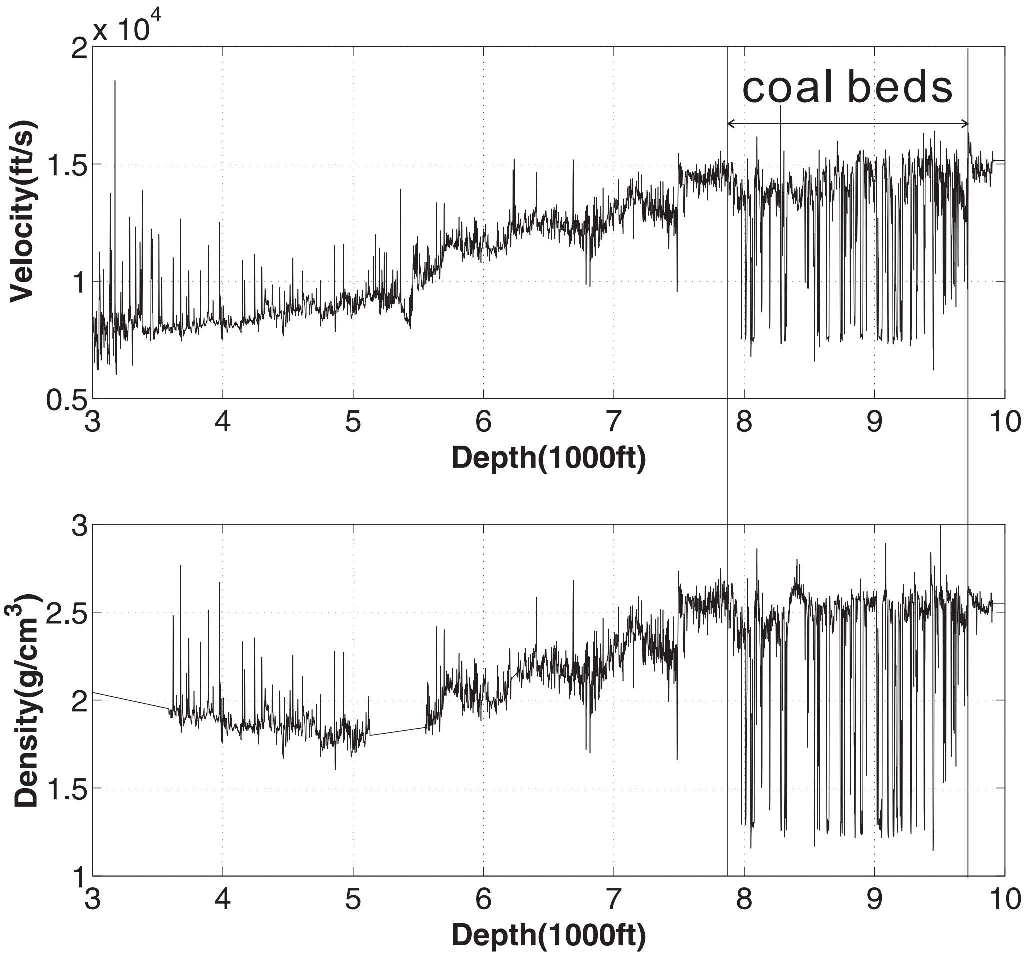

Figure 3.1: Raw well log curves.

layers in the well is about **40** among which **35** layers are thinner than $\boldsymbol{20ft}$ ($\boldsymbol{6m}$) and that means the two-way traveltime for those layers is less than $\boldsymbol{5ms}$. The thinnest coal layer measured by the well log curves is $\boldsymbol{3ft}$ ($\boldsymbol{0.9m}$) which means only $\boldsymbol{0.8ms}$ two-way traveltime. In order to accurately represent the true velocity and density of the coal beds in the time domain, a sampling interval of $\boldsymbol{1.0ms}$ is used in converting the depth logs into time for developing the synthetic seismograms.

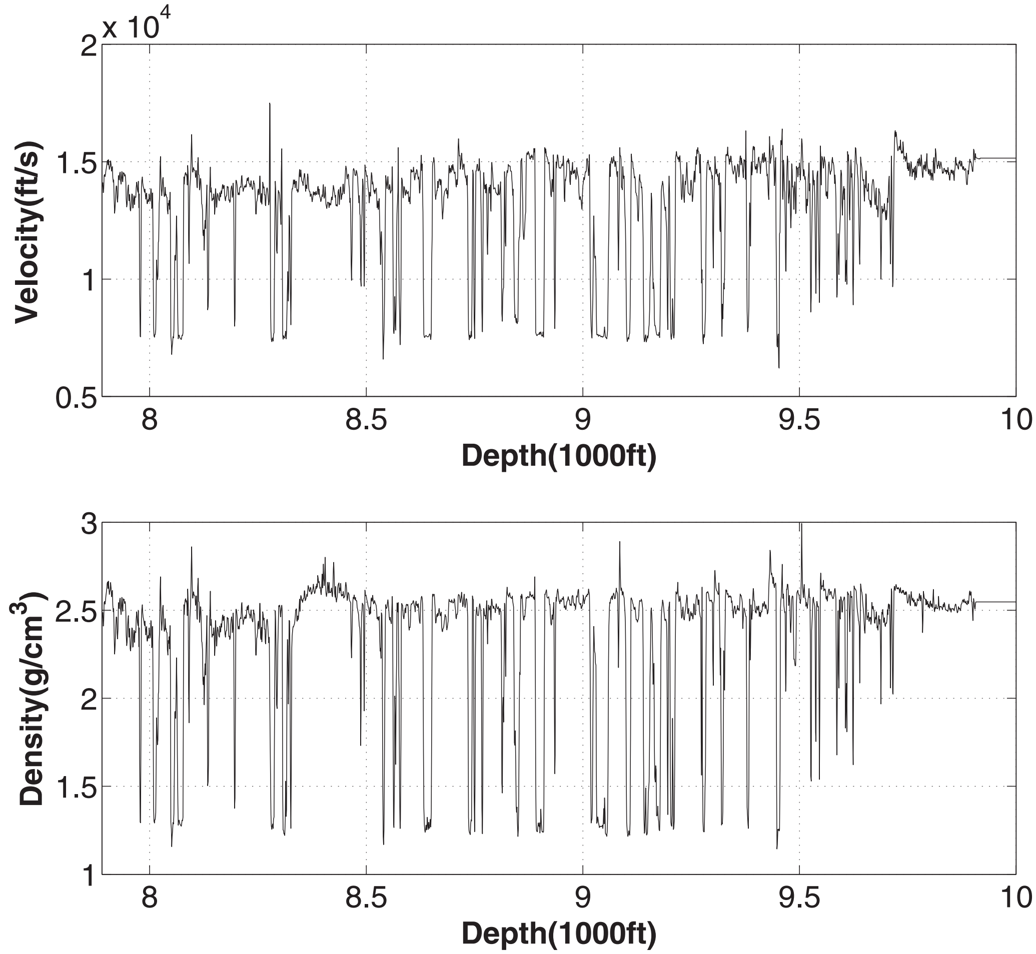

Figure 3.2: Enlarged version of well log curves in coal-bed interval.

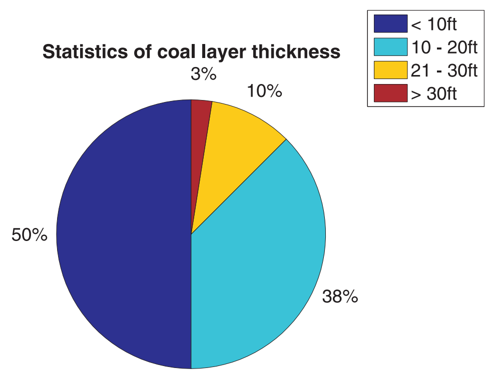

Figure 3.3: Thickness statistics of coal layers.

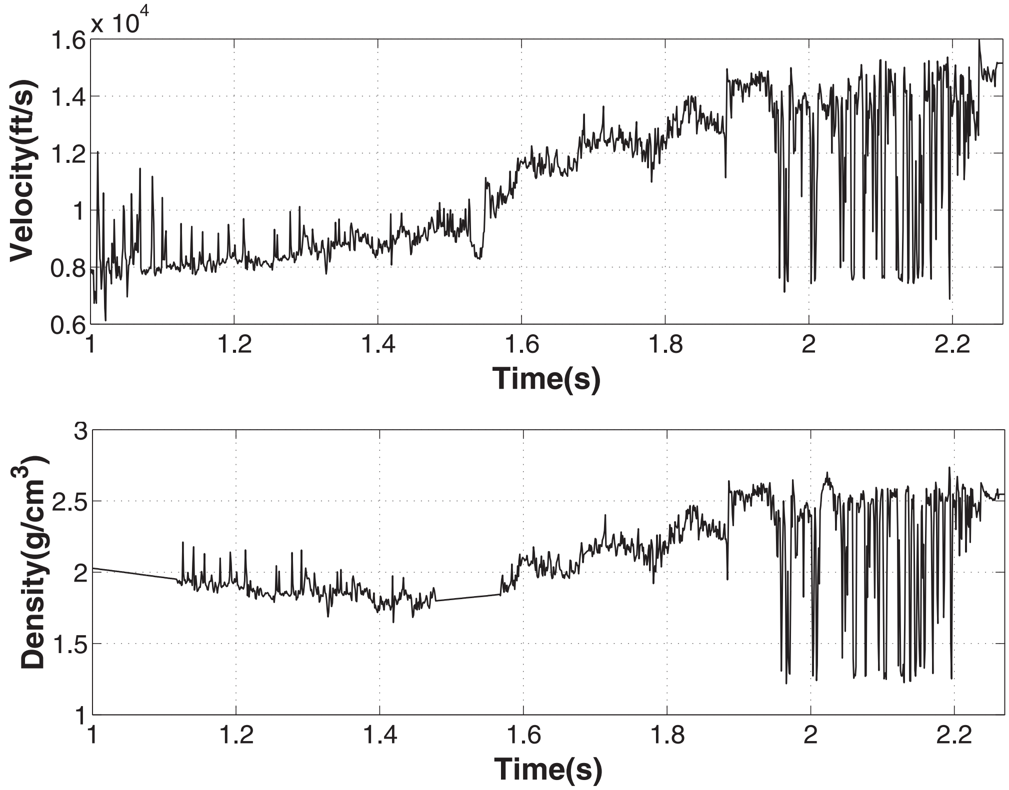

Figure 3.4: Time domain well log curves. A two-way traveltime interval of $\boldsymbol{1ms}$ is used to convert the depth logs into time logs.

3.1.2 Seismic data

A **3*D*** seismic survey that was reprocessed in **2012** crossed the well location used in this study. The seismic data were pre-stack migrated and offset-limited stacks along with full stacks were available for analyses. Initially, the well-tie was done with the full offset stack; however, because the synthetic trace is a normal incident response, a near-offset seismic stack may provide a better match to the synthetic than the full seismic stack. Figures 3.5 and 3.6 illustrate the full and near-offset stacks. An amplitude spectrum from the near-offset stack at the top of the coal beds is shown in Figure 3.7. From this spectrum an Ormsby filter was designed for the preliminary well-tie (Figure 3.8).

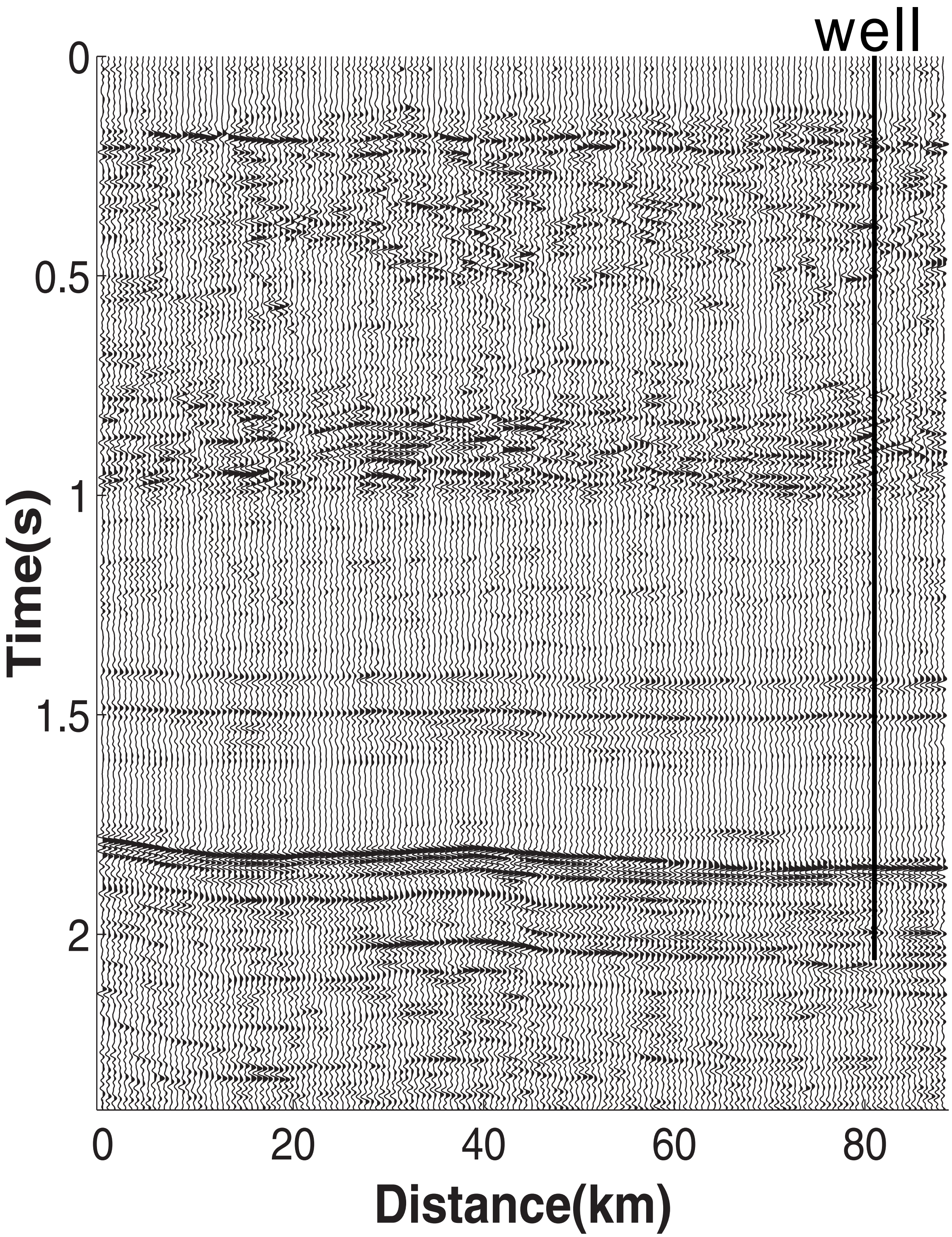

Figure 3.5: Seismic profile(full-offset stack) with well location.

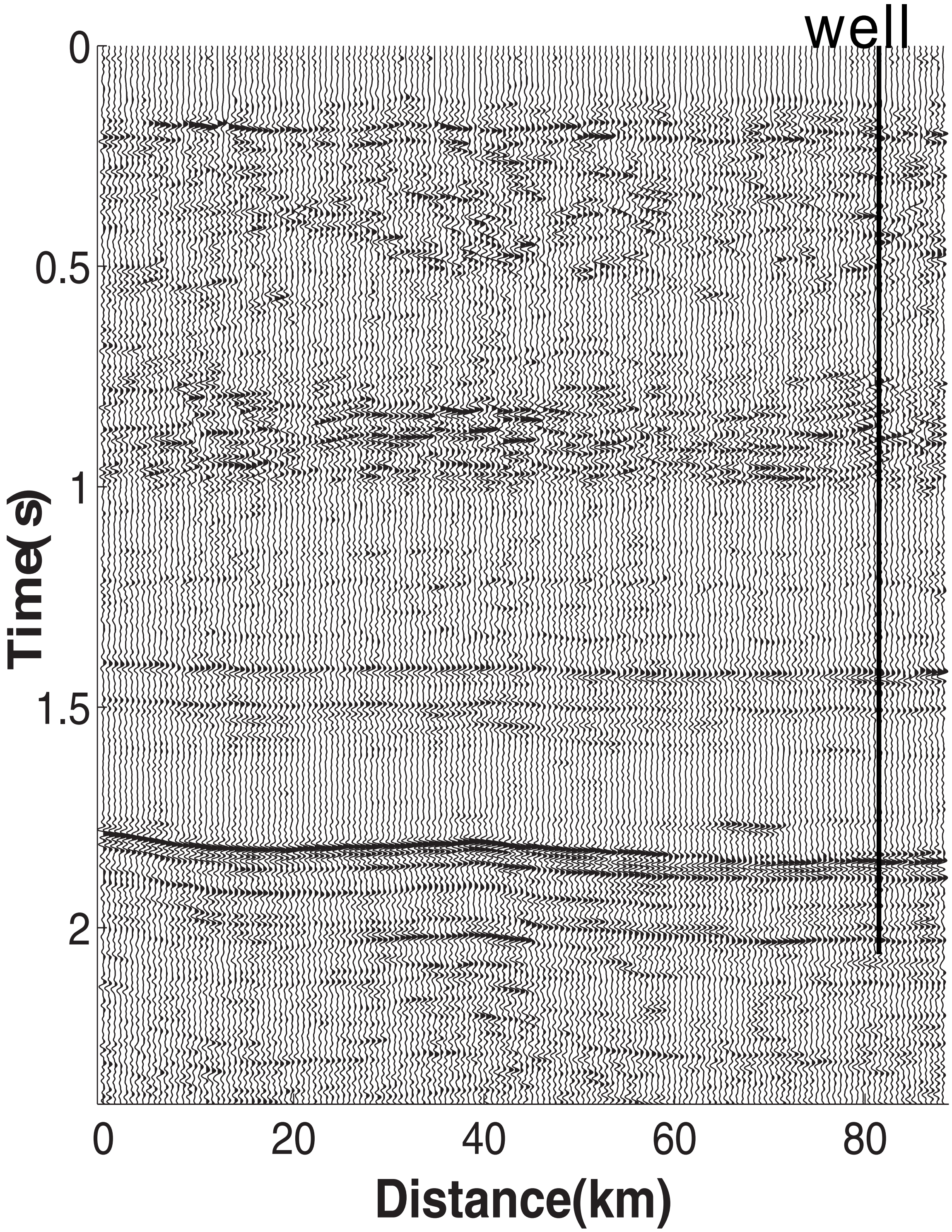

Figure 3.6: Seismic profile(near-offset stack) with well location.

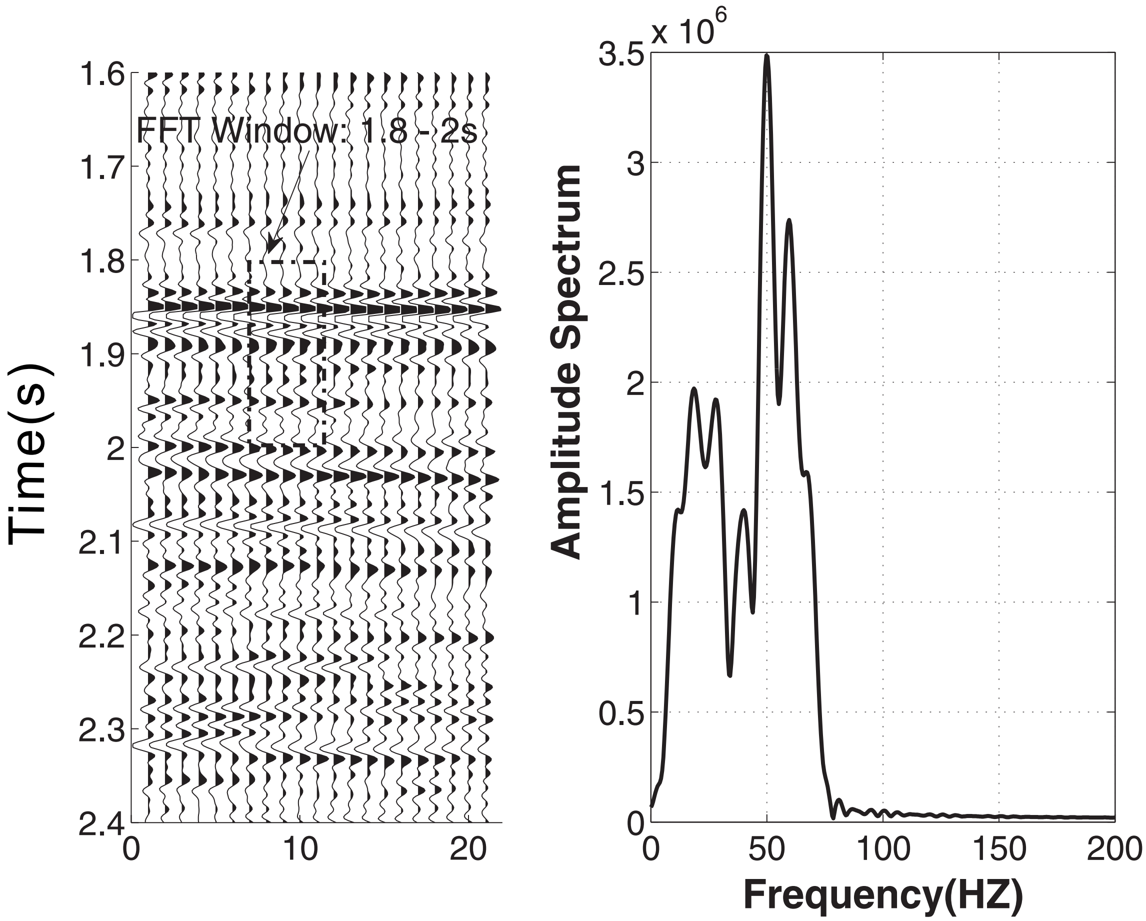

Figure 3.7: Amplitude spectrum from near-offset stack at top of coal beds.

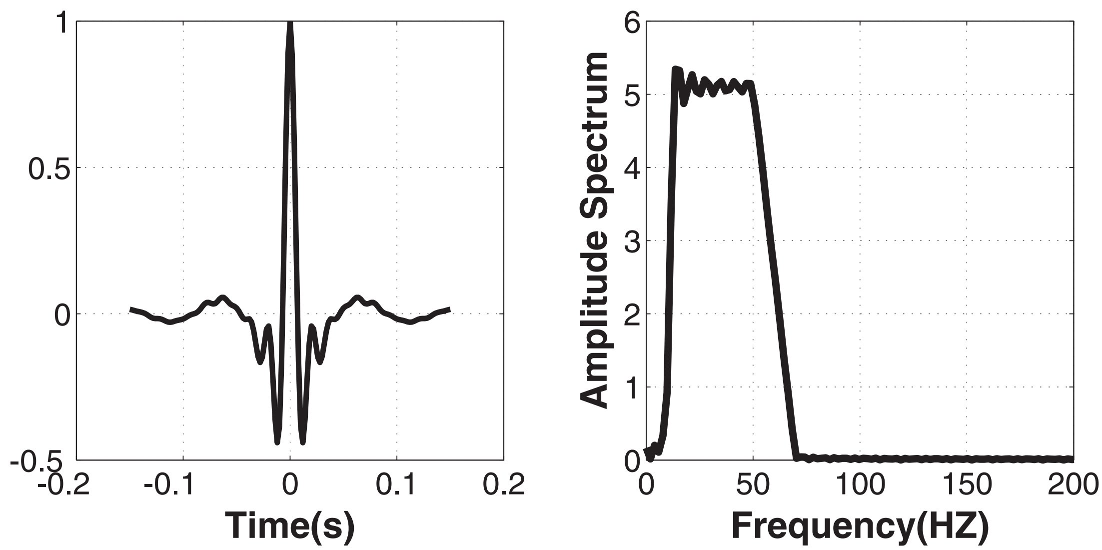

Figure 3.8: Ormsby filter with $\boldsymbol{10-12-50-70Hz}$ bandpass and zero-phase spectrum.

3.2 Well-tie

Several goals are achieved during the well-tie analysis. Firstly, attenuation effects caused by interbed multiples in the coal beds are captured by comparing the well-tie with primary-only reflections versus the primary plus multiple reflections. Secondly, the algorithm based on Waters (1981) methodology to generate a synthetic with all internal multiples is verified. Finally, since coals are known to shatter when drilled, a quality control method for the sonic log measurements is developed to revise the coal bed sonic readings.

3.2.1 Primary only synthetic versus all internal multiples synthetic

The first comparison involves two synthetics: one with primary reflections only and the other with primary reflections plus interbed multiples and this is shown in Figure 3.9.

The near-offset stack seismic profile is used and a $\boldsymbol{10-12-50-70Hz}$ zero-phase Ormsby bandpass filter (Figure 3.8) represents the source wavelet. The synthetic with primary-only reflections in Figure 3.9(a) fails to match the seismic data after $\boldsymbol{1900ms}$ while the synthetic with primary reflections and all interbed multiples resembles the seismic data but misties the seismic events after $\boldsymbol{2050ms}$. The amplitude in the primary-only synthetic at $\boldsymbol{2.0s}$ is too large compared to the seismic at the same time, while the multiple synthetic shows the correct amplitude when compared to the seismic. In fact, it appears that a little stretch on the multiple synthetic would really increase the quality of the tie to the seismic.

Backus averaging increases the apparent traveltime through the coal beds over the integrated sonic time so the synthetic with primary reflections only has a better performance after logs are Backus-averaged. A detailed description of the Backus averaging technique is given by Liner (2004). I tested averaging lengths of $\boldsymbol{30ft}$ ($\boldsymbol{9m}$) , $\boldsymbol{50ft}$ ($\boldsymbol{15m}$) and $\boldsymbol{200ft}$ ($\boldsymbol{61m}$). Figure 3.10 shows the $\boldsymbol{50ft}$ ($\boldsymbol{15m}$) Backus-averaged velocity log compared with the raw velocity log. Backus averaging decreases the extreme variations in the velocity log. The traveltime through the coal beds is increased over the measured sonic traveltime by $\boldsymbol{25ms}$ when the $\boldsymbol{50ft}$ ($\boldsymbol{15m}$)

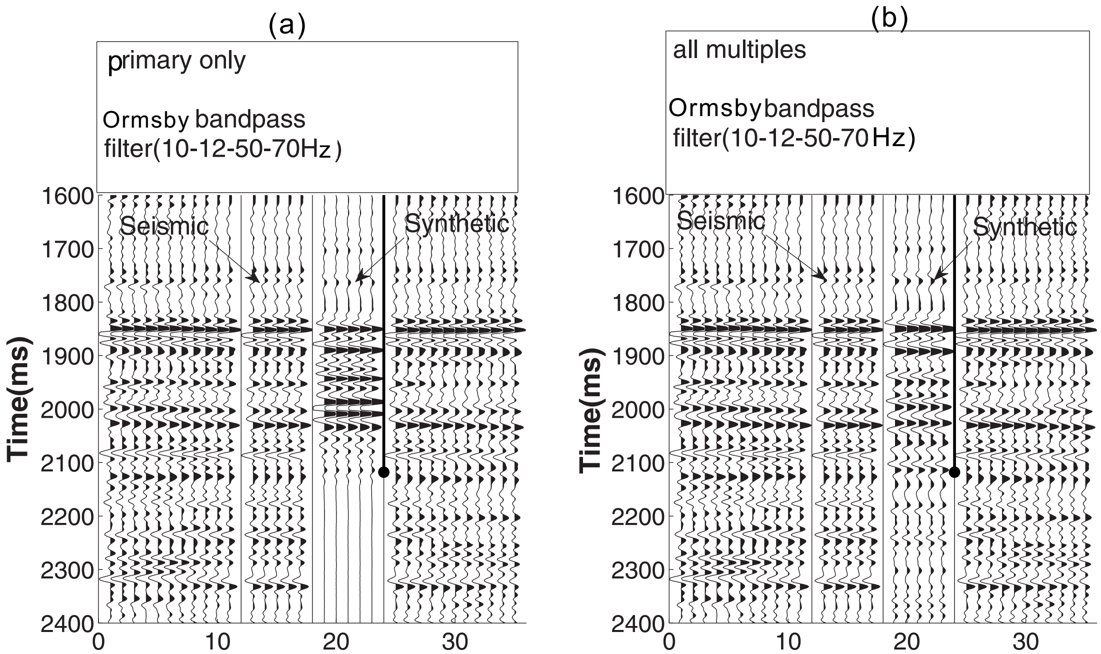

Figure 3.9: **(a)** Synthetics with primary-only reflections versus **(b)** primary reflections plus interbed multiples.

averaging is performed. Figure 3.11 compares the well-tie using synthetic trace with primary-only reflections and the well-tie using primary with multiple reflections using the $\boldsymbol{50ft}$ ($\boldsymbol{15m}$) averaging.

Backus averaging does improve the well-tie with primary-only reflections. However the synthetic with primaries and multiples still performs better than the primary-only synthetic.

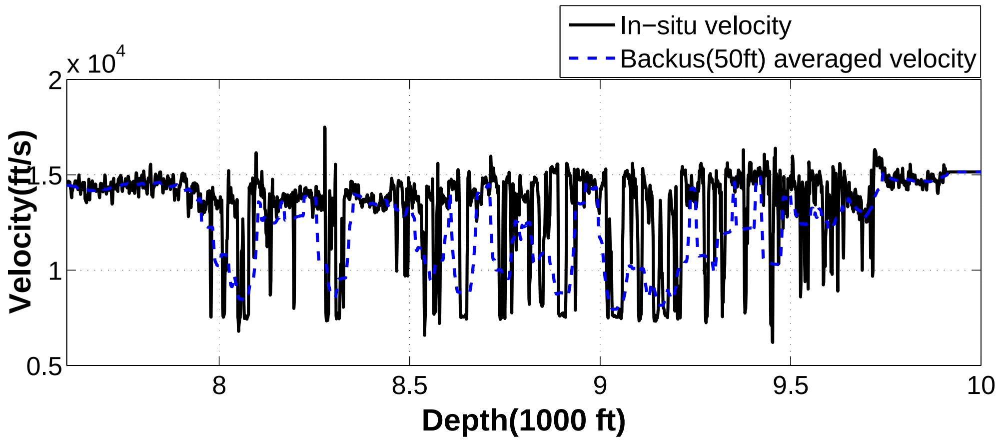

Figure 3.10: Velocity log before and after Backus averaging.

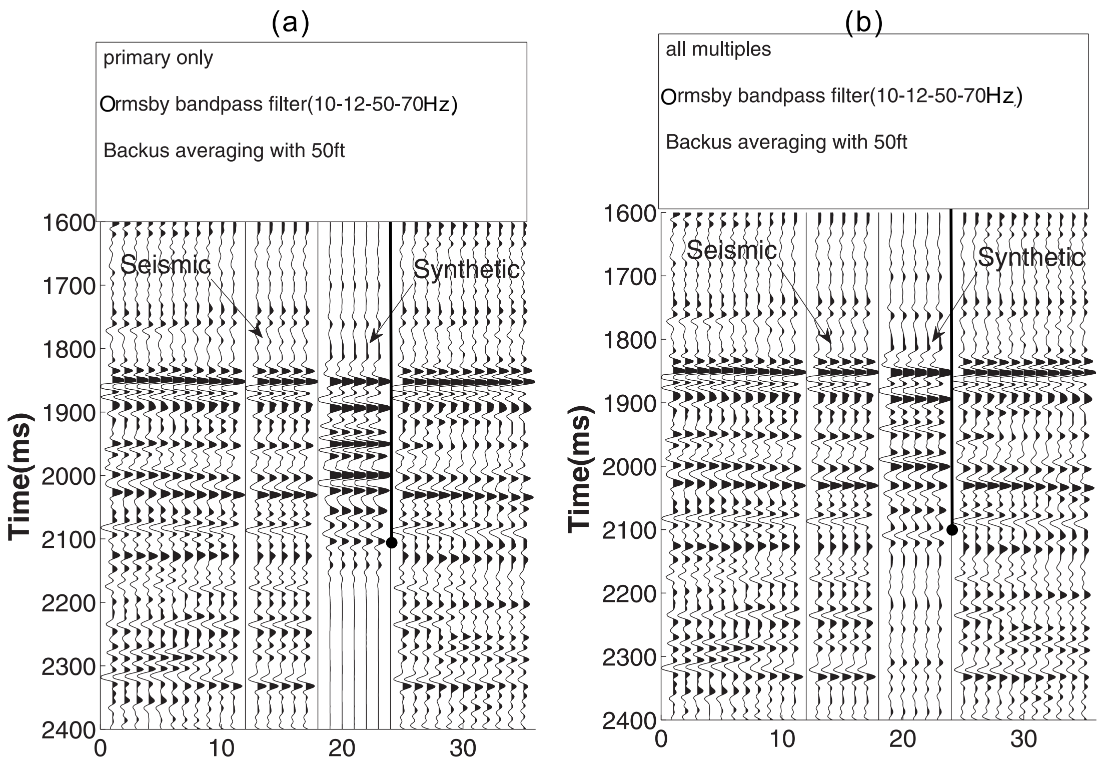

Figure 3.11: **(a)** Synthetics with primary-only reflections versus **(b)** primary reflections plus interbed multiples. Both synthetics use Backus-averaged log data.

3.2.2 Near-offset seismic stack versus full-offset stack

Because the synthetic trace is a normal incident response, a near-offset seismic stack may provide a better match to the synthetic than the full seismic stack. The synthetic trace with primaries and multiples is compared with the near-offset and full-offset stack in Figure 3.12. The near-offset stack ties better than the corresponding full-offset stack. For instance, at proximately $\boldsymbol{2020ms}$, the near-offset stack has a better correlation than the full-offset stack. So the near-offset stack is used in the following analyses.

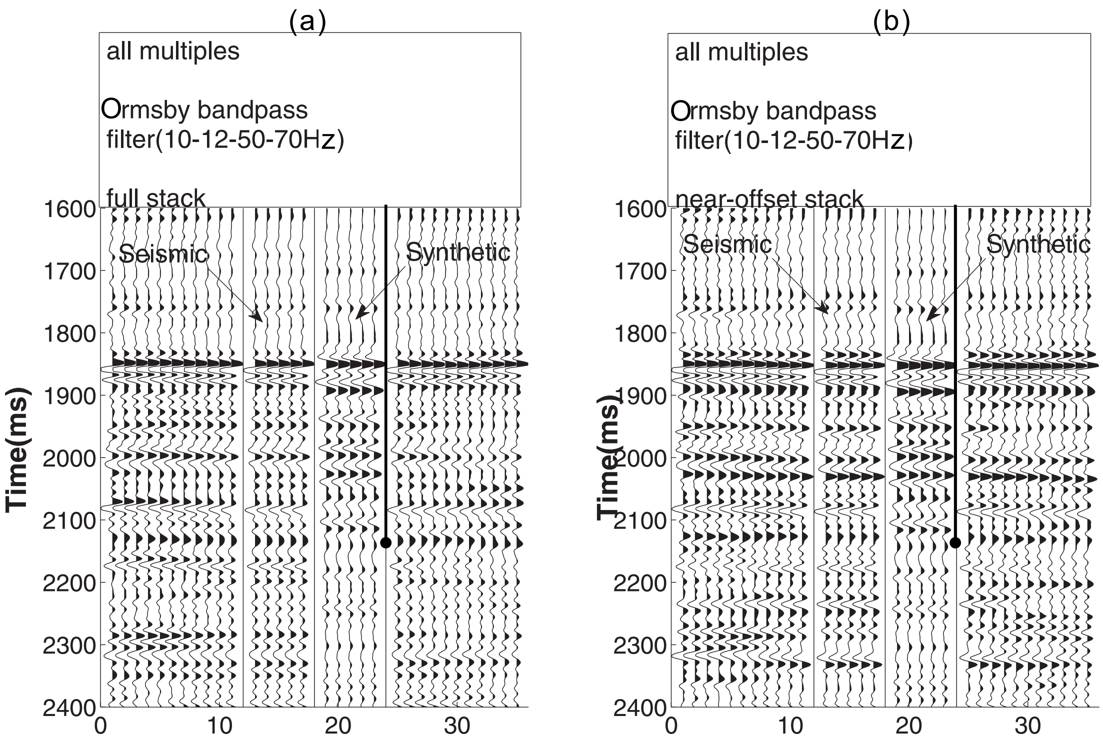

Figure 3.12: **(a)** Well ties using near-offset stack versus **(b)** full-offset stack.

3.2.3 Well log editing

Coals are known to shatter when drilled and this might contribute to the mistie that starts at $\boldsymbol{2020ms}$ in Figure 3.12(b) on the near-offset stack. The synthetic indicates that stretching might improve the tie.

If the coal formation shattered, the drilling mud could invade the formation and the measured velocity would increase. Rather than stretching the synthetic, it was reasoned that all coal beds should have the same interval velocity and thus those coal intervals that had a velocity less than $\boldsymbol{12000ft/s}$ ($\boldsymbol{3658m/s}$) in the depth domain were lowered to the $\boldsymbol{7350ft/s}$ ($\boldsymbol{2240m/s}$) as shown in Figure 3.13. This reduction in velocity would automatically stretch the synthetic trace and thus increase the chances for a better tie. The well-tie comparison between the in-situ velocity log and the modified velocity log is illustrated in Figure 3.14. The synthetic comparison to the near-offset stack in Figure 3.14(b) has improved over that shown in Figure 3.14(a). With the improved well-tie with the modified coal bed velocity log, it is used in the following analyses.

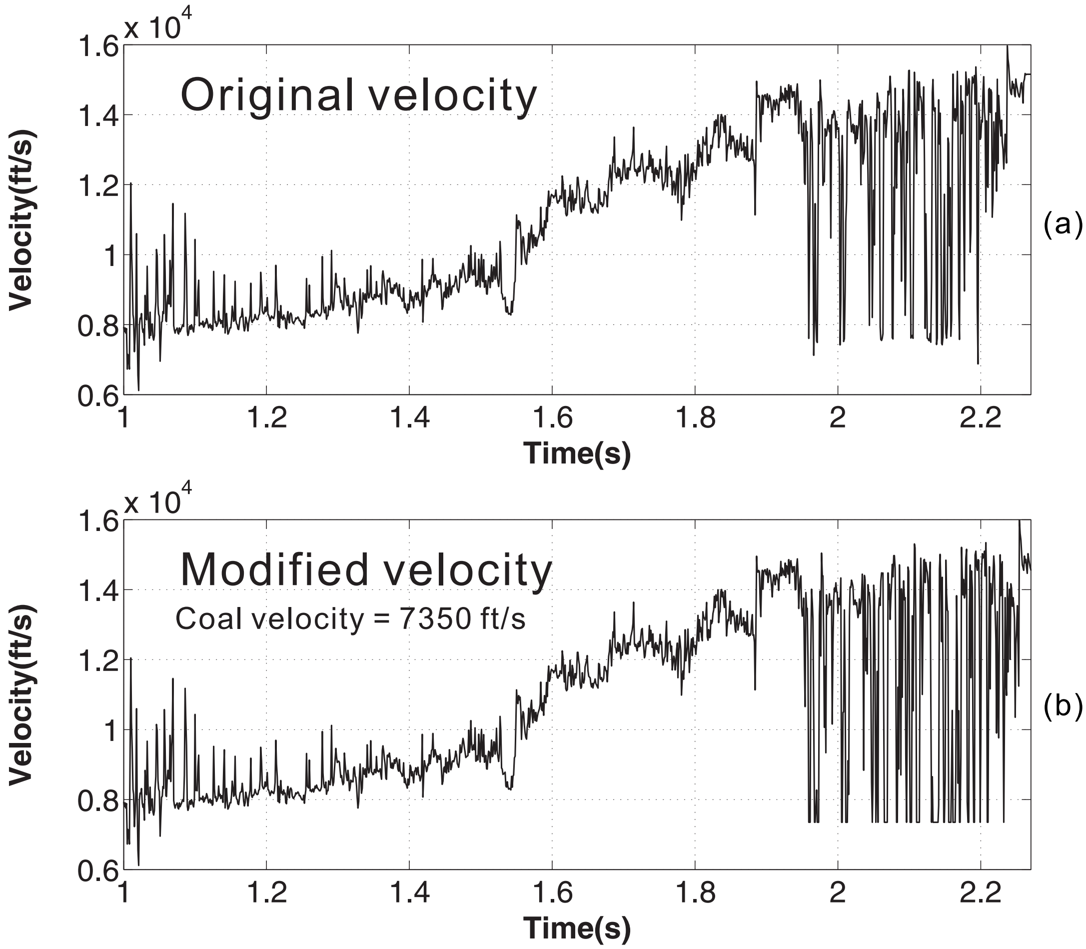

Figure 3.13: Raw velocity log versus modified velocity log with coal velocity edited to $\boldsymbol{7350 ft/s}$ ($\boldsymbol{2240 m/s}$) for all coal layers.

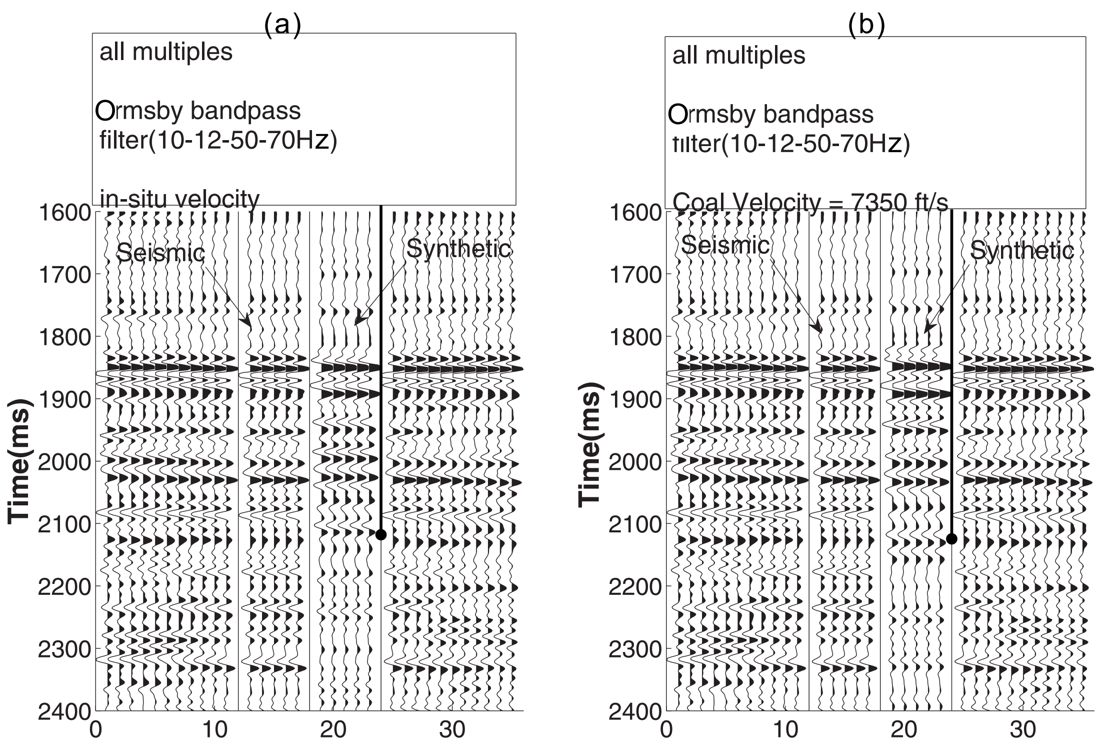

Figure 3.14: Synthetics using raw velocity log and edited velocity log. Density log is left intact.

3.2.4 Wavelet extraction

In Figures 3.9 to 3.14, it is suspected that the source wavelet is not zero phase. In order to create the best well-tie, the source wavelet, in particular the phase spectrum needs to be extracted. The wavelet extraction is done at the beginning of the coal beds using the reflectivity with primaries and multiples and the near-offset stack. Figure 3.15 illustrates the correlation window which is from $\boldsymbol{1.8s}$ to $\boldsymbol{1.96s}$. With the $\boldsymbol{160ms}$ window, a $\boldsymbol{100ms}$ wavelet is extracted and truncated with a trapezoidal filter that has the weights of $\boldsymbol{(0, 1, 1, 0)}$ at the times of $\boldsymbol{(-50ms, -24ms, 24ms, 50ms)}$. A 5-point smoothing filter then is applied on the extracted wavelet. The wavelet and its spectra are shown in Figure 3.16.

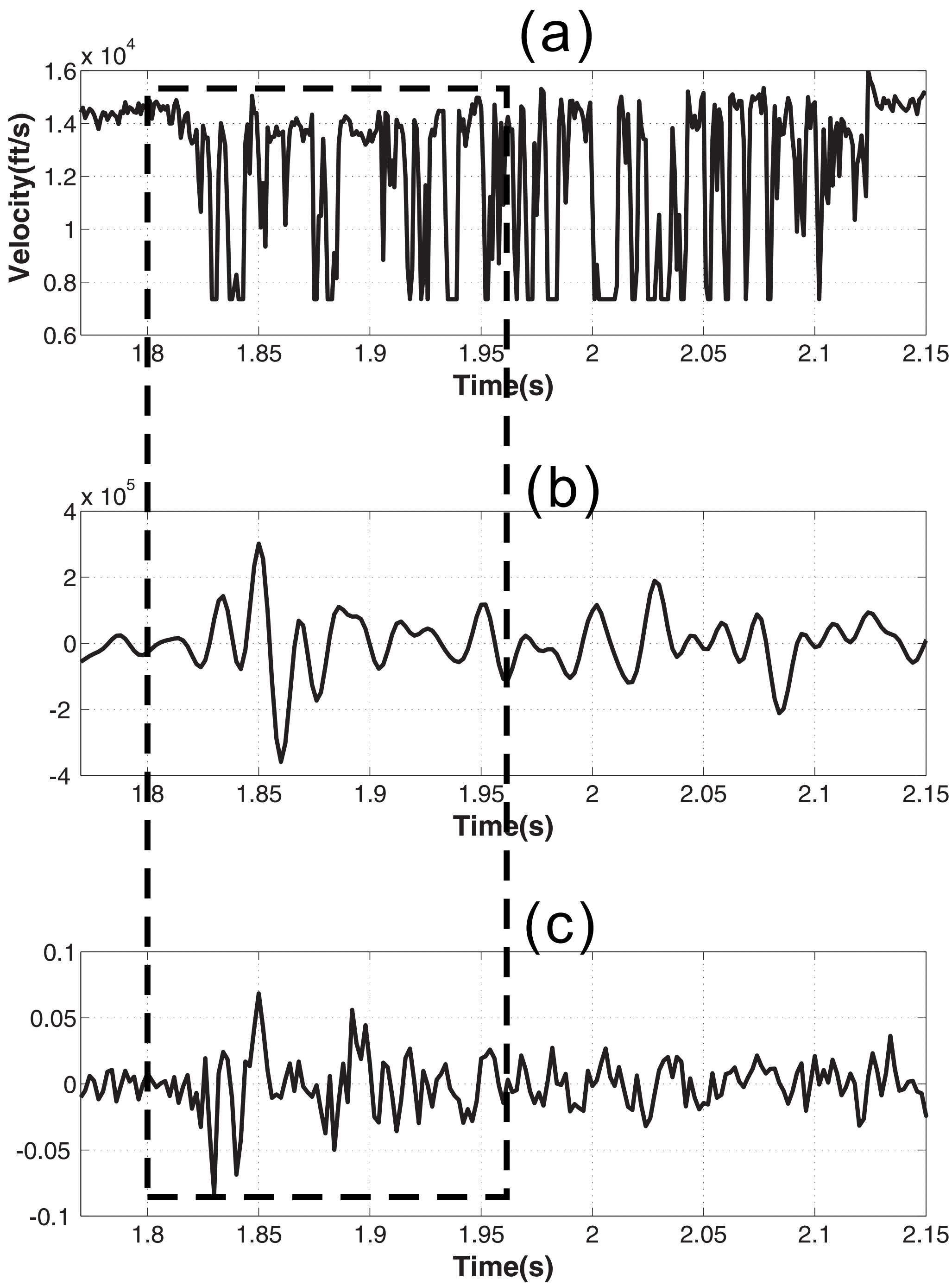

Figure 3.15: Wavelet extraction window. The $\boldsymbol{160ms}$ window is located at the beginning of coal beds. **(a)** Velocity log, **(b)** seismic trace, and **(c)** multiple synthetic with impulse source.

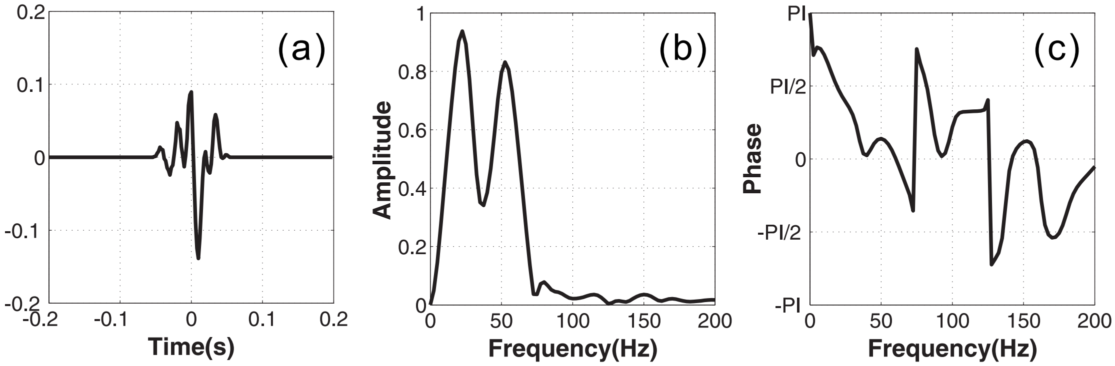

Figure 3.16: Source wavelet extracted by least-squares method. **(a)** Extracted wavelet, **(b)** amplitude spectrum, and **(c)** phase spectrum of the wavelet.

3.2.5 Summary and the best well-tie parameters

From the well-tie tests, several conclusions are obtained. The algorithm based on Waters (1981) is verified with the good well-tie when the coal velocity is modified to $\boldsymbol{7350 ft/s}$ ($\boldsymbol{2240 m/s}$). The well-tie is enhanced by using an extracted wavelet,which essentially applies a phase rotation, and the resulting well-tie is shown in Figure 3.17.

The edited well log will be carried forward to be used in generating the wavelet dictionary which is contaminated by interbed multiples and a $\boldsymbol{40 Hz}$ Ricker wavelet will be used as the source wavelet in the following study in order to avoid interpretation difficulties introduced by the asymmetry of the extracted wavelet (Figure 3.16).

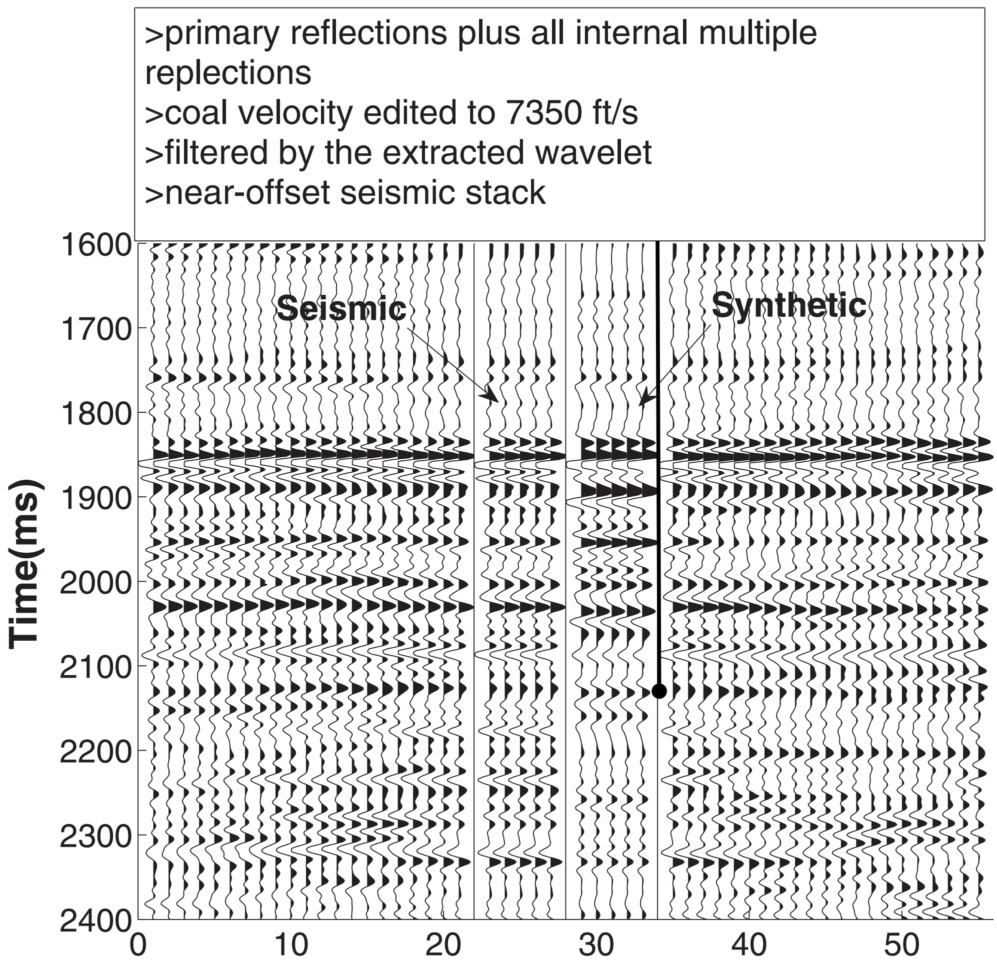

Figure 3.17: The best well-tie using the parameters listed in the top text box.

3.3 Processing goal: nonstationary deconvolution of wavelet dictionary

3.3.1 Wavelet dictionary computed from the well

Margrave (1997) proposed that any nonstationary but linear effect could be included into the nonstationary model by the appropriate modification of the convolutional matrix $\boldsymbol{w(\tau, t-\tau)}$ in the nonstationary convolution equation (equation 1.3). A method for modifying the wavelet dictionary that reflects the filtering effects caused by interbed multiples has been discussed in **Chapter 2**.

The primary-only normal-incident reflection coefficients represent the earth model reflection coefficient series and the wavelet dictionary represents the time-varying source wavelets. For this example, the wavelet dictionary is $\boldsymbol{600ms}$ and is shown in Figure 3.18. Each column in the wavelet dictionary represents a propagating wavelet whose arrival time is related to the column number. For example, if seismic sampling rate is $\boldsymbol{1ms}$, the $\boldsymbol{k'th}$ column in the wavelet dictionary represents the propagating wavelet with the arrival time of $\boldsymbol{k(ms)}$. The effects of the multiples are incorporated only in the propagating wavelet as the reflection coefficient column in the nonstationary convolution matrix contains primaries only.

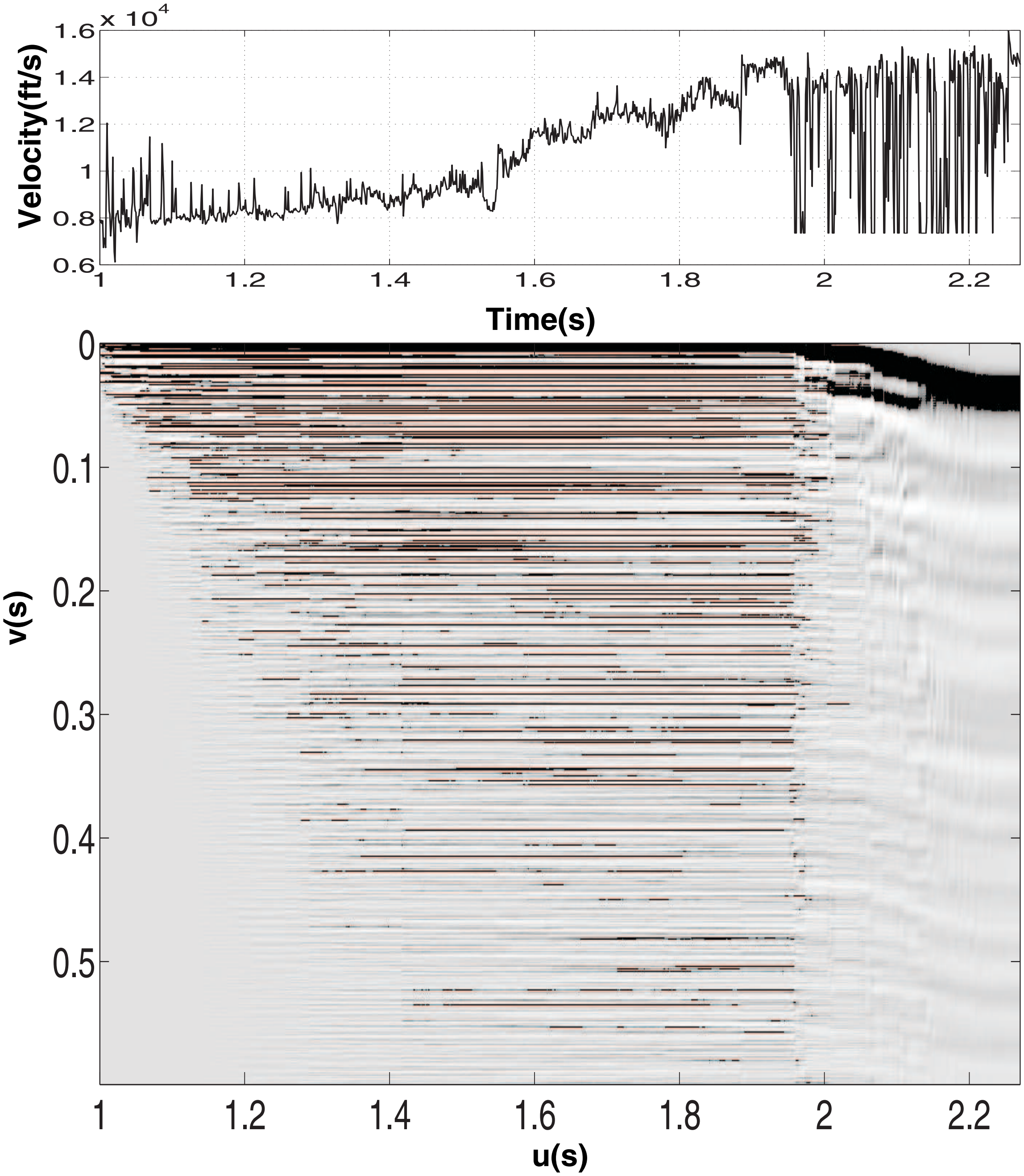

Figure 3.18: Wavelet dictionary computed based on edited velocity log and raw density log. $\boldsymbol{u}$ and $\boldsymbol{v}$ have the same meanings as they appear in Margrave (1997): $\boldsymbol{u}$ denotes arrival time of an impulse reflection and $\boldsymbol{v}$ denotes time in each wavelet relative to its arrival time($\boldsymbol{u}$). Notice the frequency change in the coal beds.

3.3.2 Nonstationary convolution between wavelet dictionary and reflection coefficients

Based on equation 1.3 and its matrix form illustrated in Figure 1.2 , nonstationary convolution with the wavelet dictionary matrix and the reflection coefficient column matrix yields the synthetic seismogram with internal multiples. This is illustrated in Figure 3.19 without the source wavelet applied. The stationary source wavelet could be added by convolving the source wavelet with the reflection coefficient column vector or with each column in the wavelet dictionary matrix. Figure 3.20 shows the nonstationary convolution process when the wavelet dictionary matrix is convolved with a $\boldsymbol{40Hz}$ Ricker wavelet.

Because the output trace by nonstationary convolution reflects attenuation effects caused by interbed multiples , it is requisite to compare the nonstationary convolution output with the synthetic seismic trace with primary and multiple reflections as calculated by Waters (1981) algorithm.

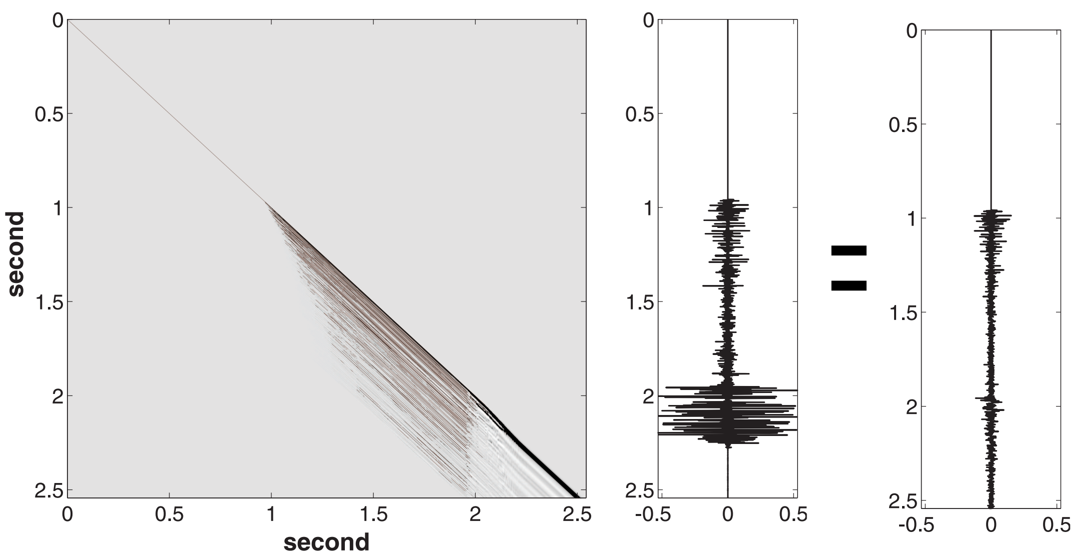

Figure 3.19: Nonstationary convolution as a matrix multiplication. The convolutional matrix is the time shifted wavelet dictionary which reflects the attenuation effects caused by interbed multiples. The source is an impulse.

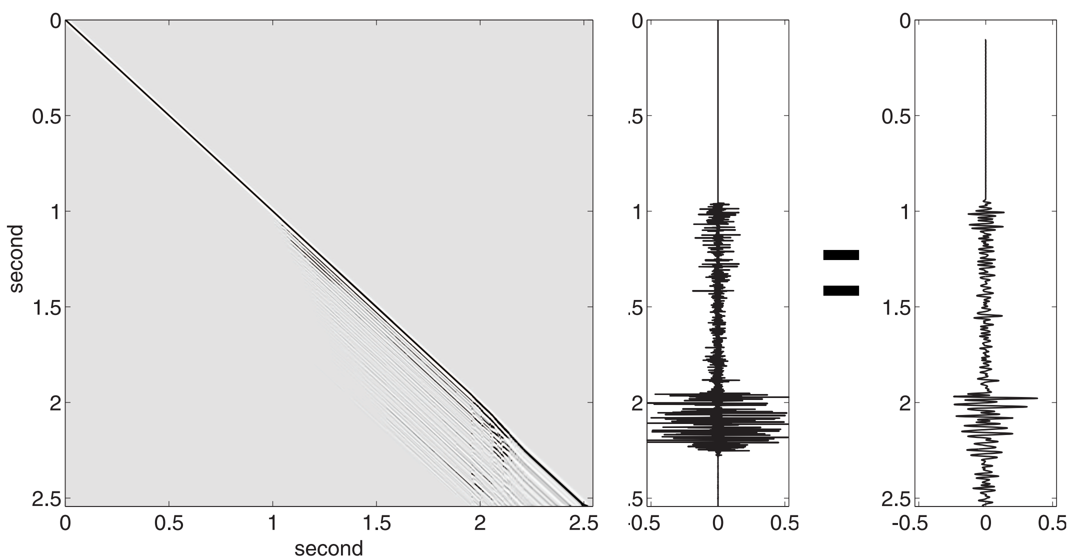

Figure 3.20: Nonstationary convolution using the same wavelet dictionary convolved with a $\mathbf{40}\boldsymbol{Hz}$ Ricker-source wavelet. The same output vector could be reached by convolving the source wavelet with the reflection coefficient column on the right side.

3.3.3 Waters' primary and multiple synthetic versus wavelet dictionary synthetic

Figure 3.21 compares the synthetics computed with Waters algorithm (black solid curve) versus the synthetic generated with the wavelet dictionary and the primary reflection coefficient series (orange dash curve) with the same $\boldsymbol{40Hz}$ Ricker source wavelet. The perfect match between the two traces validates the wavelet dictionary approach of computing synthetics with multiples.

If the wavelet dictionary can be defined, then there is a possibility of applying time-varying deconvolution operators to suppress the multiples or at least suppress the broadening of the propagating wavelet as it travels through the coal beds. The wavelet dictionary approach is cartooned below where the wavelets in the dictionary are different in each column (Figure 3.22). The deconvolution is also cartooned below (Figure 3.23).

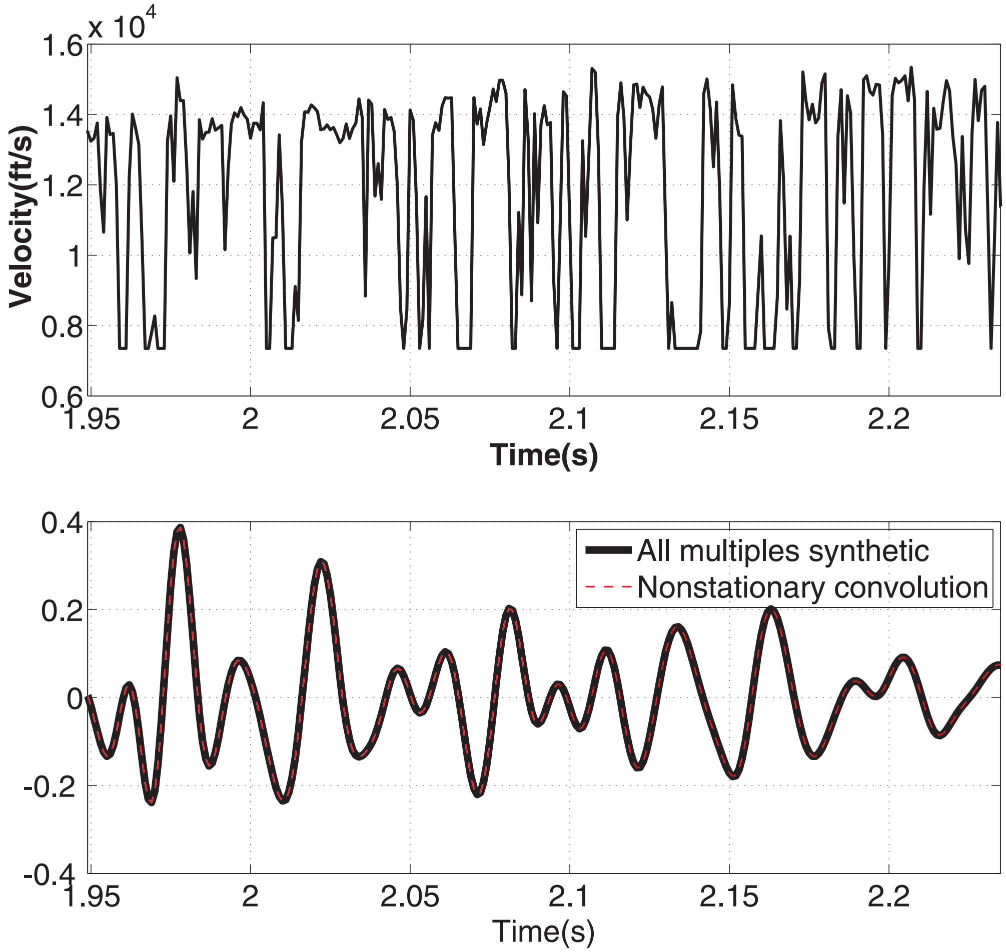

Figure 3.21: Comparison between the synthetic with primaries and multiples computed with Waters algorithm versus a synthetic computed as a convolution of the wavelet dictionary with the primary reflection coefficients. A $\mathbf{40}\boldsymbol{Hz}$ Ricker-source wavelet is convolved with each trace.

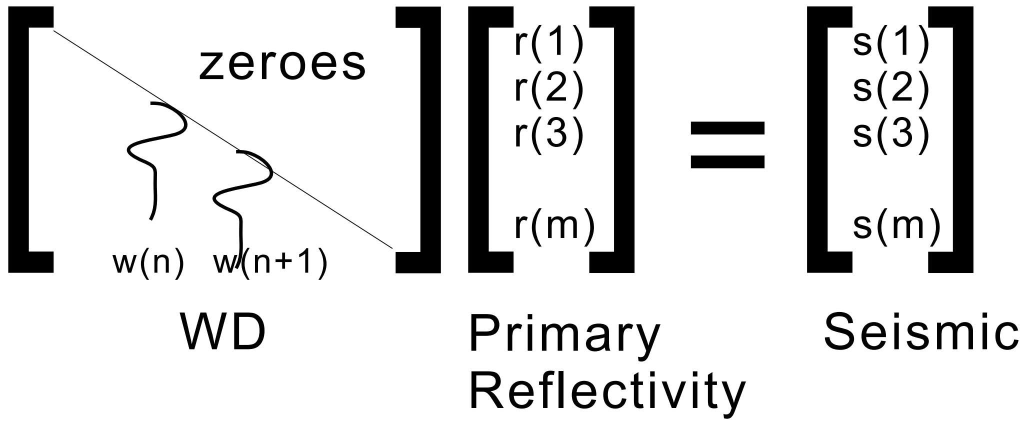

Figure 3.22: Illustration of wavelet dictionary in nonstationary convolution.

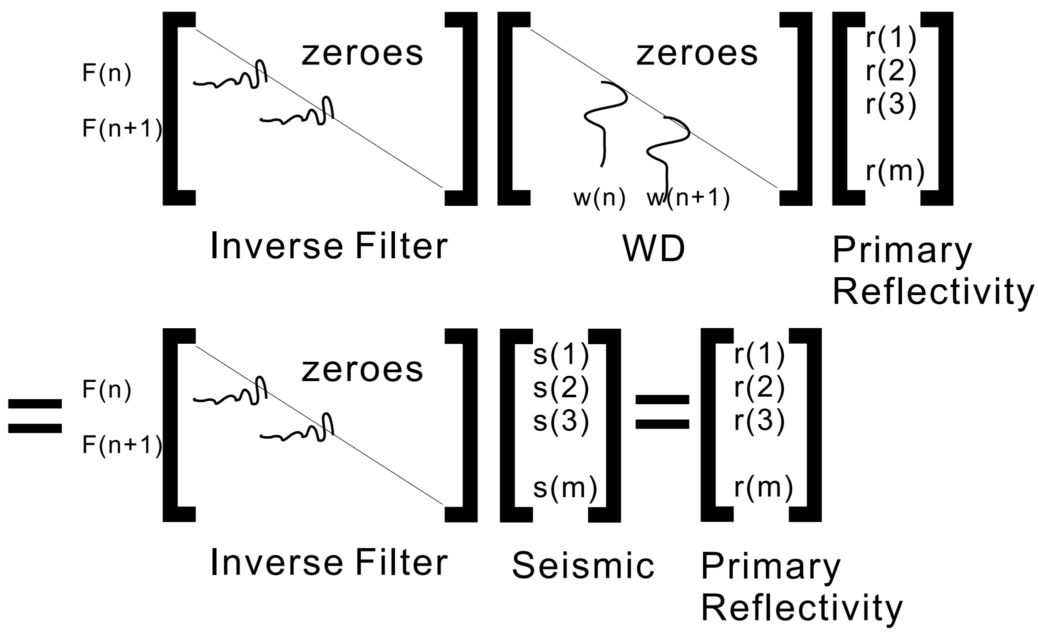

Figure 3.23: Illustration of the process to inverse filter the multiple effects.

In the second cartoon, a time-varying inverse filter has been applied to the seismic trace $\boldsymbol{s}$, in such a fashion that the final output is the desired reflection coefficient series with primary events only, that is, no multiples. Numerous authors have suggested that the propagating wavelet is minimum-phase and as such, its inverse filter will be a one-sided minimum-phase filter. The design of the inverse filters is out of the scope of this research. What will be considered is how the wavelet dictionary might be defined from seismic field data.

3.4 Attenuation effects caused by interbed multiples

3.4.1 High-frequency filtering and time delays derived from the wavelet dictionary

As shown in the previous section, the synthetic in the coal beds can be viewed as a nonstationary convolution of the wavelet dictionary with the primary reflection coefficients.

As such, the attenuation of the propagating wavelet received at the surface can be understood by the studying of the wavelet dictionary. Figure 3.24 shows wavelets in the wavelet dictionary at various positions with respect to the coal beds. Trace **1900** represents the propagating wavelet whose arrival time is $\mathbf{1900}\boldsymbol{ms}$ because the sampling rate of the refection coefficient series is $\mathbf{1}\boldsymbol{ms}$. It represents the surface

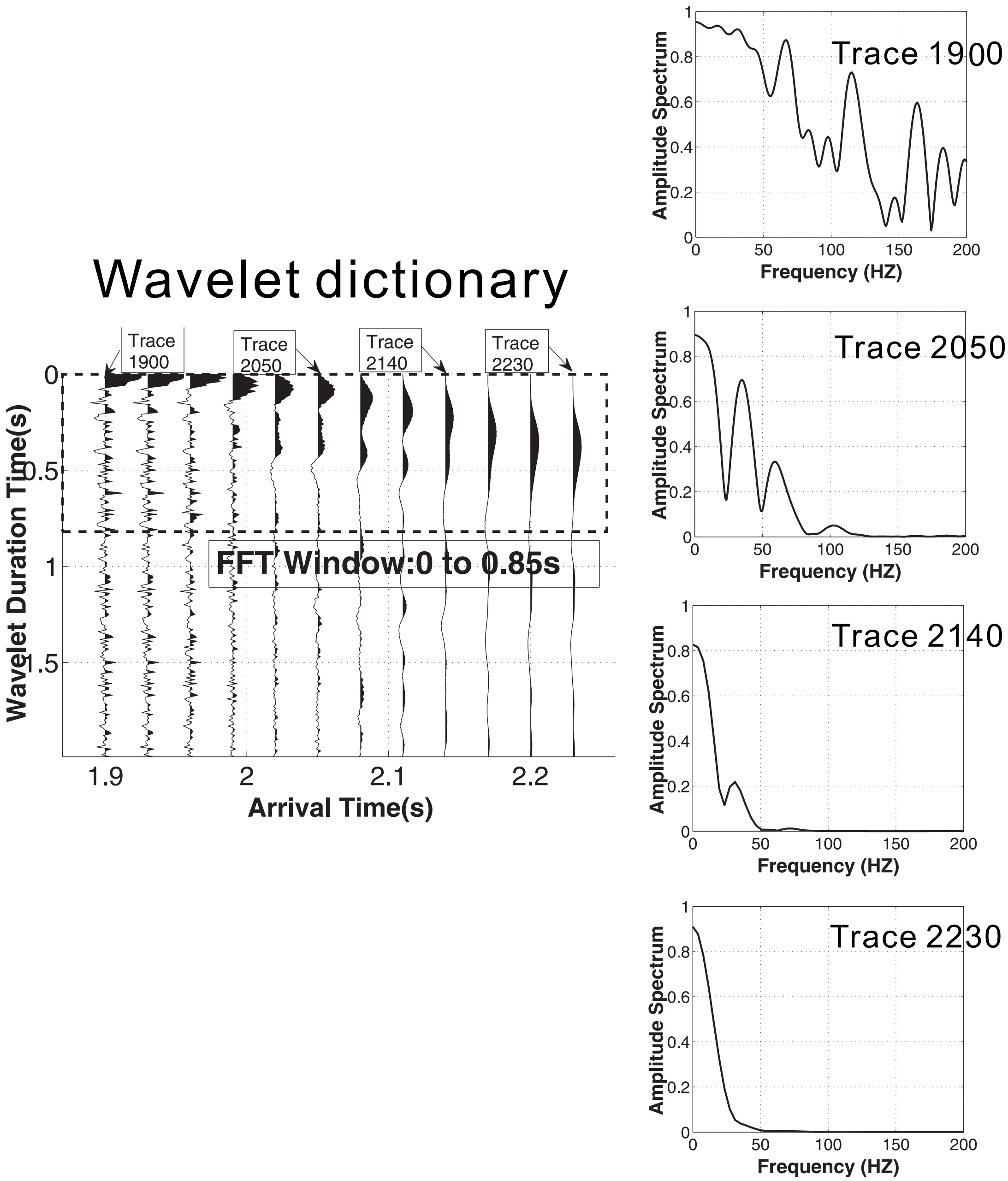

Figure 3.24: The spectra of wavelets in wavelet dictionary.

received propagating wavelet reflected at an interface above the coal beds and trace **2230** represents the surface received propagating wavelet reflected at the bottom of coal beds. As noted in the accompanying spectra, the high-frequency content in the wavelet decays quickly from trace 1900 to trace 2230. The high-frequency decay reinforces the conclusions made by O'Doherty and Anstey(1971) and Schoenberger and Levin(1974).

A final observation from Figure 3.24 is that the amplitude spectra are shaped to a narrow low-frequency curve that resembles a Gaussian function.

The first sample value for each wavelet in wavelet dictionary represents the primary reflection and as shown in Figure 3.24, the first sample amplitude decreases quickly after trace **1900** while the maximum amplitude in each wavelet slowly decays. These observations coincide with the conclusion made by O'Doherty and Anstey (1971) where in particular, the interbed multiples tend to preserve the amplitude of seismic reflections. By picking the time arrival of the maximum amplitude for each wavelet in the wavelet dictionary, a curve is generated that represents the time delay effects caused by interbed multiples as mentioned by Stewart et al. (1984). The time delay curve is plotted in Figure 3.25. The horizontal axis indicates the arrival time of the primary reflections and it is easy to see at the end of coal beds, the maximum energy in each wavelet is delayed by $\boldsymbol{38ms}$ compared to its primary reflection arrival time. The coal beds are from $\boldsymbol{7974ft}$ to $\boldsymbol{9457ft}$ ($\boldsymbol{2430-2882m}$) (MD), so the delay trend is $\boldsymbol{25.6ms/1000ft}$ ($\boldsymbol{304m}$) which is about twelve times larger than the delay trend of $\boldsymbol{2.0ms/1000ft}$ ($\boldsymbol{304m}$) derived from the non-coal sediments of Oklahoma and East Texas (Stewart et al., 1984).

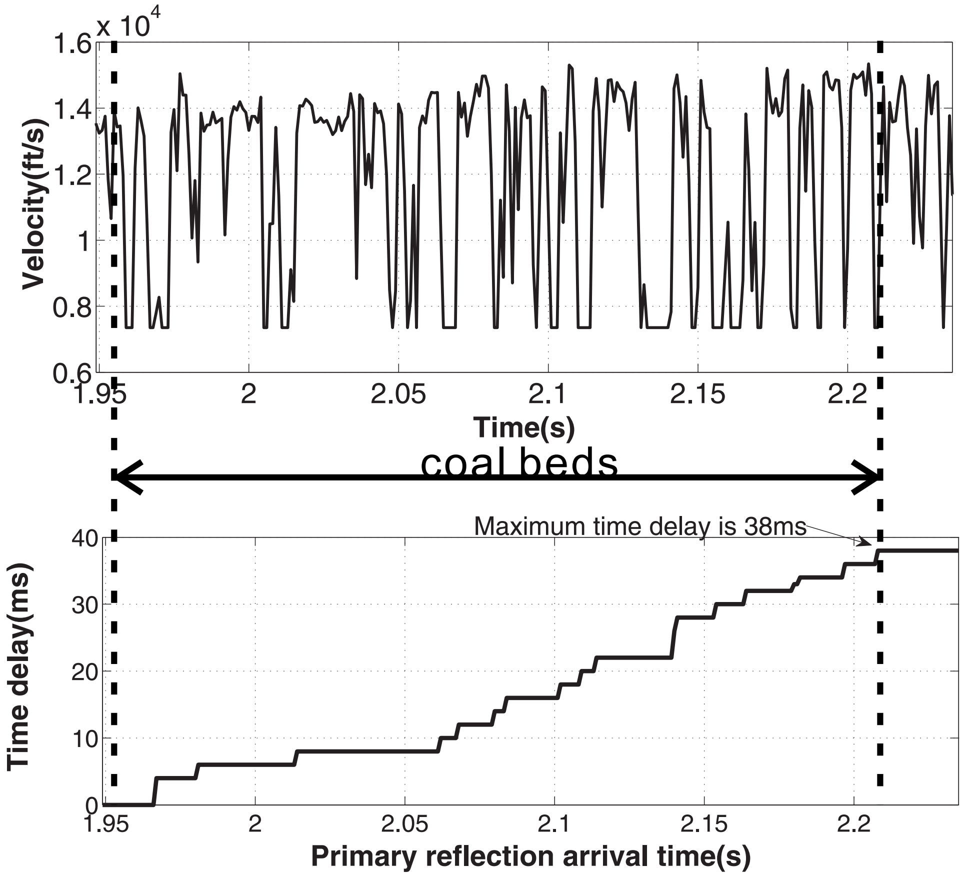

Figure 3.25: Time delay trend from arrival times of the maximum amplitude of the wavelets in wavelet dictionary.

3.4.2 Primary-only transmission loss versus transmission loss from wavelet dictionary

Interbed multiples tend to preserve energy in reflections (O'Doherty and Anstey, 1971). Standard transmission loss is computed as

$$\boldsymbol{T_n = (1 - r_2^2)(1 - r_3^2)...(1 - r_n^2),} \tag{3.1}$$

where $\boldsymbol{T_n}$ represents the primary-only transmission loss in the $\boldsymbol{n'th}$ layer and $\boldsymbol{r_n}$ represents the reflection coefficient at the $\boldsymbol{n'th}$ interface. The energy loss for primary reflections is then computed as

$$\boldsymbol{EL_n = 10log_{10}T_n^2 = 20log_{10}T_n.} \tag{3.2}$$

The energy loss for wavelets in wavelet dictionary is defined as

$$\boldsymbol{\tilde{E}L_n = 10log_{10}\sum_n W_n^2,} \tag{3.3}$$

where $\boldsymbol{\sum_n W_n^2}$ represents the sum of the squared amplitudes in the $\boldsymbol{n'th}$ column of wavelet dictionary. $\boldsymbol{EL_n}$ (dashed curve) and $\boldsymbol{\tilde{E}L_n}$ (solid curve) are plotted in Figure 3.26.

The energy loss changes dramatically for primary reflections once the waves travel into the coal beds. The coal beds cause up to $\boldsymbol{110dB}$ loss to the primary reflections at the base of coal bed interval. However, a much smaller energy loss of $\boldsymbol{12dB}$ is observed for the wavelets in the WD at the base of the coal beds. This observation coincides with the conclusion by O'Doherty and Anstey (1971).

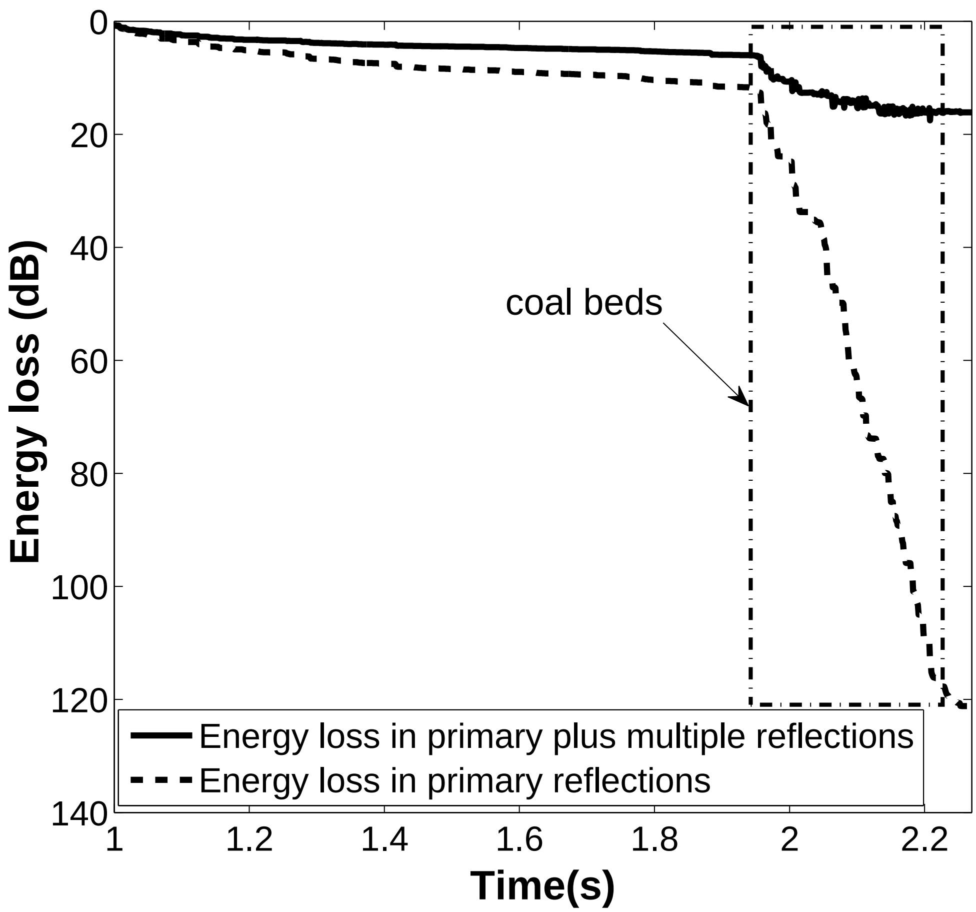

Figure 3.26: Different rates of energy decay with and without the consideration of multiples. The energy in primary-only reflections decays faster than that from the primary plus all internal multiple reflections.

3.4.3 Seismic vertical resolution in coal beds

Seismic resolution is decreased greatly by interbed multiples from coal beds and even below the coal bed sequences, a single layer can't be identified unless it is significantly deeper than the last coal layer. This section analyzes these effects and proves that the effects are not only because of the high-frequency attenuation of the wavelets but also are affected greatly by the shallower interbed multiples from the beginning of coal beds.

Three coal layers are selected to test seismic vertical resolution (Figure 3.27). For each coal layer, two synthetics with all internal multiples are computed and compared. One synthetic uses well log curves from the surface to just above the top of the studied coal layer while the other synthetic uses well log curves from the surface to just below the specified coal layer.

Seismic modeling based on the stationary convolutional model and the nonstationary convolutional model is also tested to determine if there are any advantages for using the nonstationary convolutional model. For stationary convolutional modeling, ignore (set to zero) all reflection coefficients outside the studied coal layer and convolve (equation 1.2) the reflection coefficients in the studied layer with the constant source wavelet. For nonstationary convolutional model, use the same reflection coefficients in the studied layer and convolve the reflection coefficients with the nonstationary wavelets in WD.

Using layer 1 as an example, the resolution result is illustrated in Figure 3.28(a) and the seismic modeling is illustrated in Figure 3.28(b). In Figure 3.28(a), the black

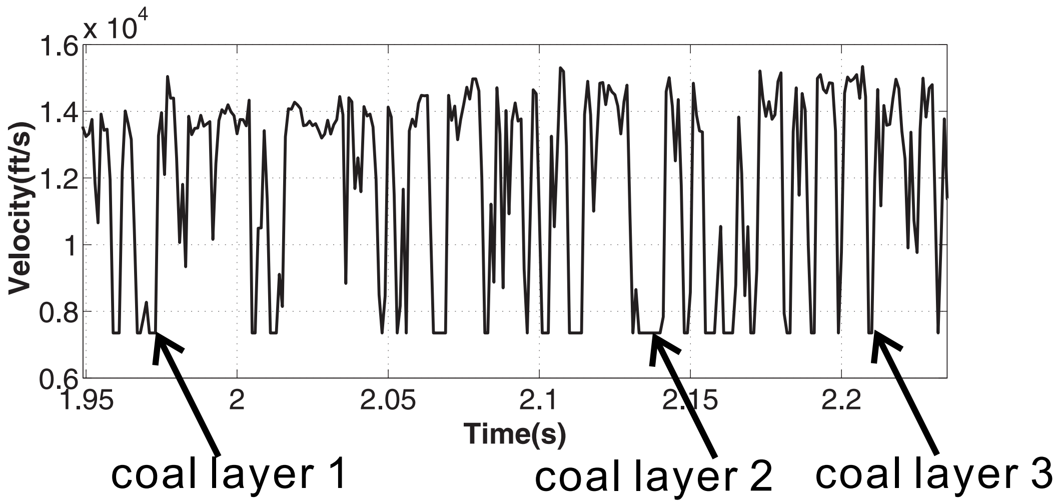

Figure 3.27: Illustration of the three coal layers studied.

solid curve and the mauve reflection coefficient stems are for the synthetic that stops just above coal layer 1; the red dashed curve and the black reflection coefficients stems are for the synthetic that stops just beneath the base of coal layer 1. If the two synthetics are almost identical, then the coal layer will be invisible with single-fold seismic. It is doubtful that multi-fold seismic would increase the ability to see coal bed because of the small moveout between primaries and internal multiples with offset.

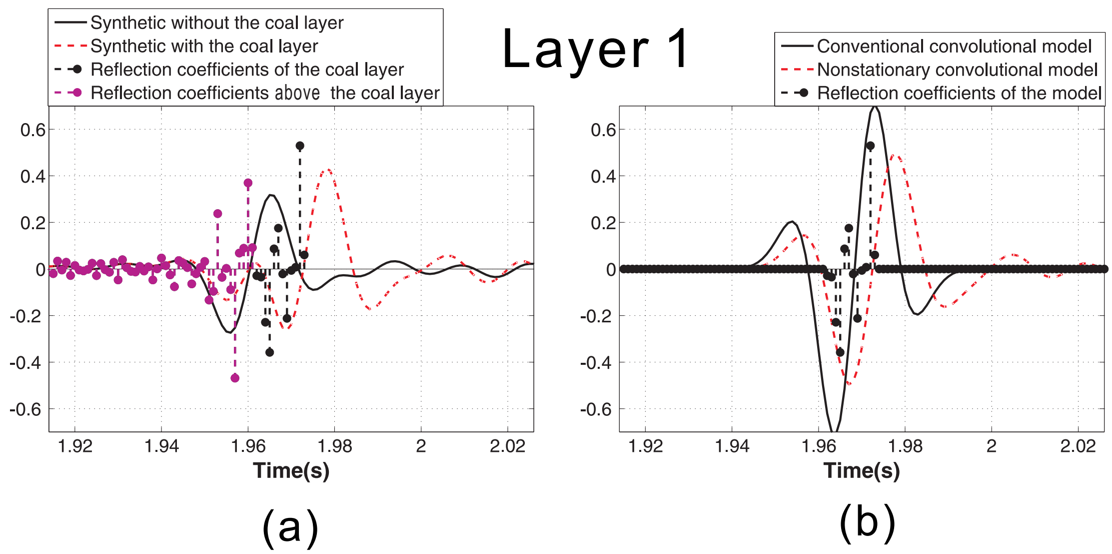

Figure 3.28: The synthetics relate to coal layer 1. **(a)** Comparison between the all multiples synthetic adding coal layer 1 in the model and the all multiples synthetic ignoring coal layer 1 in the model. **(b)** Comparison between the convolutional modeling using stationary source wavelet and the convolutional modeling using nonstationary propagating wavelet.

For each test, a $\boldsymbol{40Hz}$ Ricker wavelet represents the source wavelet. One concern is the possible dipole effect caused by the convolution between the source wavelet and the broadened wavelets in the WD. Because wavelets from the end of the coal beds have a lower frequency than the source wavelet, the convolution may yield two obvious bumps at the beginning and end of the broadened wavelet from the WD rather than one wavelet positioned at the center of the broadened wavelet. This effect will affect the accuracy to pick the arrival time for reflections from the studied layer. To illustrate the possible effect of two wavelets appearing from a single reflection, a wavelet from the WD is extracted and convolved with Ricker wavelets with varied dominant frequencies. A preliminary test is shown for this effect in Figure 3.29. An $\boldsymbol{80Hz}$ Ricker wavelet will generate a second peak with the amplitude $\boldsymbol{1/4}$ to the first peak at time $\boldsymbol{0.16s}$ while the $\boldsymbol{40Hz}$ Ricker wavelet will only generate a little bump at $\boldsymbol{0.19s}$. So, the $\boldsymbol{40Hz}$ Ricker wavelet used in the test avoids the dipole effect in the convolution and should be used with confidence.

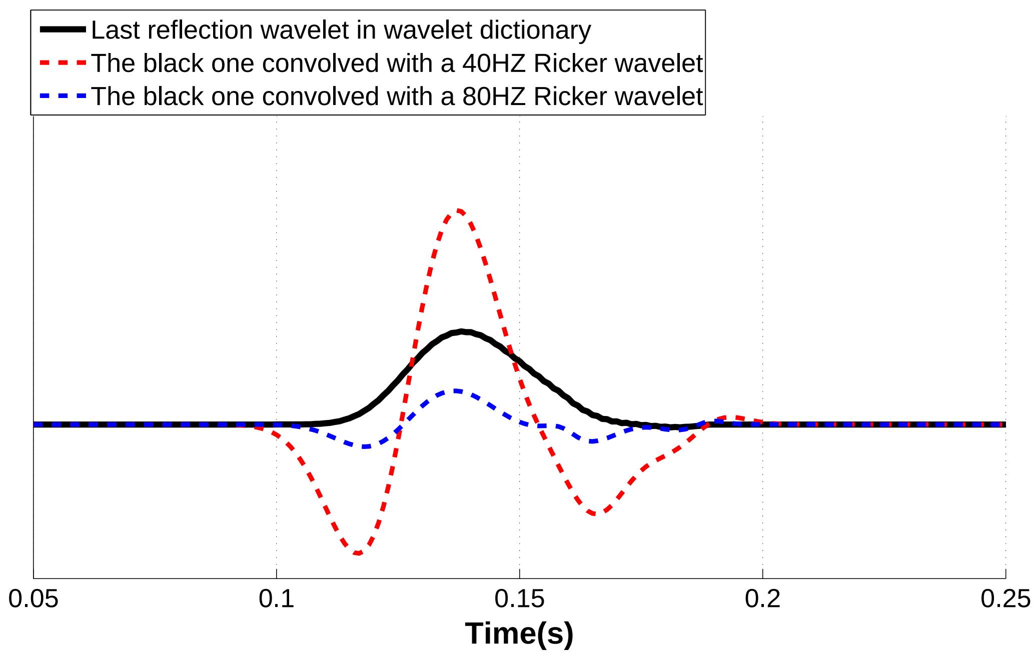

Figure 3.29: Preliminary test for possible dipole effects caused by broad reflection wavelet in wavelet dictionary convolved by a higher frequency Ricker wavelet.

Figures 3.28 to 3.31 show the results for the tests of seismic vertical resolution.

Figure 3.28 illustrates the test for layer 1. Layer one is a $\boldsymbol{12ms}$ two-way traveltime coal layer from $\boldsymbol{1964ms}$ to $\boldsymbol{1976ms}$. There is a coal bed above layer 1 that generates a strong trough-peak response as shown by the black curve in Figure 3.28(a), which is the synthetic without layer 1. The separation between the top of the coal beds above layer 1 and the top of layer 1 is approximately the same time separation between the trough and peak on the solid black curve. This means when coal layer 1 is added, coal layer 1 response will be approximately $\boldsymbol{180^\circ}$ out-of-phase with the response of the coal bed above it, thus canceling a significant portion of the upper coal bed response. In addition, both coal beds can be treated as thin beds with coal layer 1 being twice as thick as the coal bed above it. This means the amplitude response from coal layer 1 will be above twice as large as the response for the layer above it. This example illustrates the difficulty in associating troughs or peaks with specific coal beds. However, since the synthetics with and without coal layer 1 are different, coal layer 1 will be recognized as causing a change in the seismic response; although the interpretation might be difficult.

In Figure 3.28(b), the nonstationary convolutional modeling(red dashed curve) has a $\boldsymbol{7ms}$ delay for the peak at $\boldsymbol{1.971s}$ in the stationary convolutional modeling(black solid curve). From the above discussion, interbed multiples at shallow parts of coal beds delay the arrival time while wavelet broadening effects are not evident.

Figure 3.30 illustrates the test for layer 2. It is a $\boldsymbol{14ms}$ thick coal layer from $\boldsymbol{2130ms}$ to $\boldsymbol{2144ms}$, which is in the middle of the coal bed sequence. The two

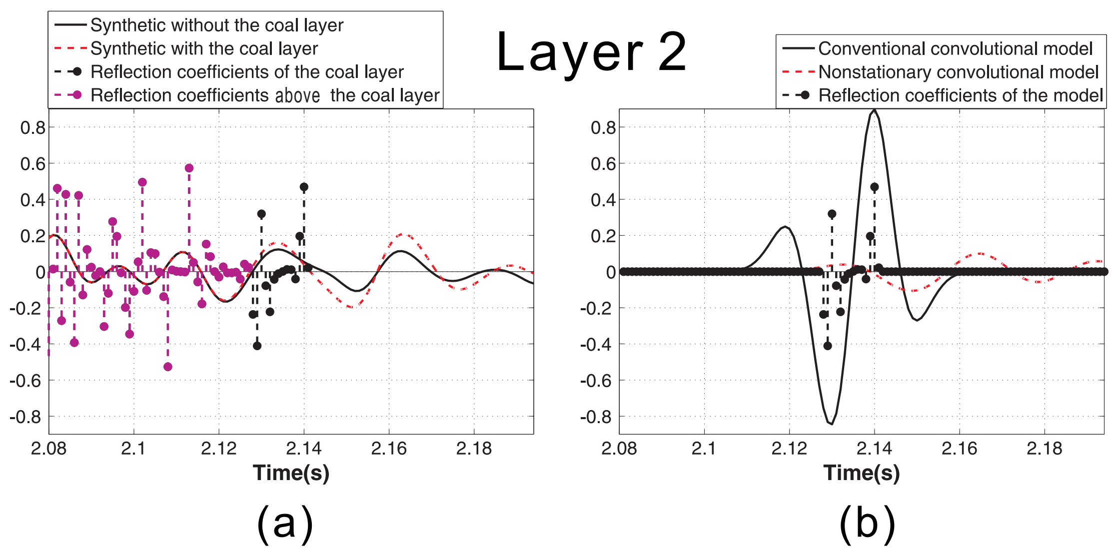

Figure 3.30: The synthetics relate to coal layer 2. **(a)** Comparison between the all multiples synthetic adding coal layer 1 in the model and the all multiples synthetic ignoring coal layer1 in the model. **(b)** Comparison between the convolutional modeling using stationary source wavelet and the convolutional modeling using nonstationary propagating wavelet.

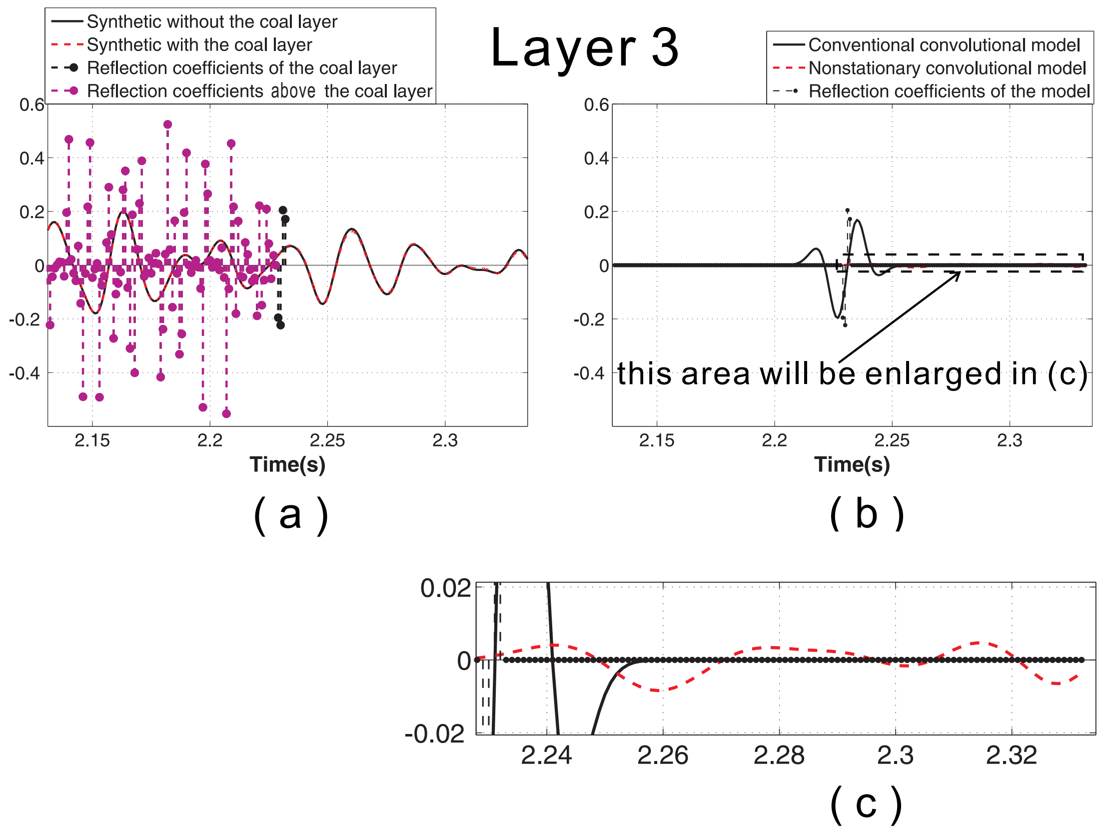

Figure 3.31: The synthetics relate to coal layer 3. **(a)** Comparison between the all multiples synthetic adding coal layer 1 in the model and the all multiples synthetic ignoring coal layer1 in the model. **(b)** Comparison between the convolutional modeling using stationary source wavelet and the convolutional modeling using nonstationary propagating wavelet.

synthetics in Figure 3.30(a) only show minor differences in the amplitude at $\mathbf{2.15}\boldsymbol{s}$, $\mathbf{2.164}\boldsymbol{s}$ and $\mathbf{2.178}\boldsymbol{s}$. It indicates that the coal layers in the middle of the coal bed sequence become more and more difficult to be distinguished even if they are relatively thick. To understand these minor differences, seismic modeling is shown in Figure 3.30(b). The true response for layer 2 (red curve) has a much lower magnitude than the conventional modeling (black curve) and is time delayed by $\mathbf{24}\boldsymbol{ms}$. Layer 3 with $\mathbf{4}\boldsymbol{ms}$ two-way traveltime at the end of coal beds is studied. The layer is totally invisible in the synthetics in Figure 3.31(a). The seismic modeling using nonstationary helps interpret the invisibility of the coal layer. On one hand, the amplitude of wavelets decay greatly at the end of coal beds due to transmission loss; on the other hand, the reflection from the end of the coal beds is noisy because of interbed multiples generated by shallower coal beds.

The tests on the three coal-bed layers prove the decrease of seismic vertical resolution as waves go into the coal beds. It is almost impossible to locate thin coal layers in the zero-offset seismic trace.

3.4.4 Seismic vertical resolution beneath coal beds

A series of tests were conducted to determine the impact of interbed multiples on the seismic resolution beneath the coal beds. The method used in the tests is similar to the previous three layers tests. A synthetic with multiples is generated for the model illustrated in Figure 3.32 and then a second synthetic is generated without the low velocity layer after the time distance "**d**". Again, nonstationary convolutional modeling will assist in the interpretation of the results.

As the time **d** is increased from $\mathbf{100}\boldsymbol{ms}$ to $\mathbf{5000}\boldsymbol{ms}$, the appended coal layer is more distant from the impact of interbed multiples which gets weaker. Figures 3.33 to 3.36 illustrate the tests conducted for **d** values of $\mathbf{100}\boldsymbol{ms}$, $\mathbf{1000}\boldsymbol{ms}$, $\mathbf{1500}\boldsymbol{ms}$ and $\mathbf{5000}\boldsymbol{ms}$ respectively.

As shown in Figure 3.33, when **d** equals $\mathbf{100}\boldsymbol{ms}$, the appended coal layer is close to the bottom of coal beds, reflections from the appended coal layer are difficult to

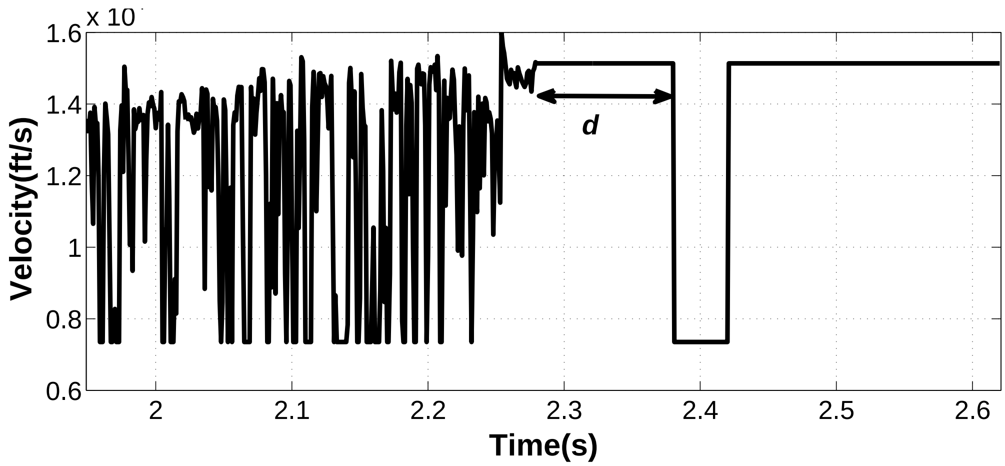

Figure 3.32: Introduction of the log model used in studying seismic vertical resolution beneath coal beds. $\boldsymbol{d}$ denotes the time interval between the studied layer and the bottom of measured well log.

identify among the interbed multiples. The synthetic with and without the appended coal layer are very similar except at times of $\boldsymbol{2.419s}$ and $\boldsymbol{2.46s}$. To explain the slight amplitude differences, the nonstationary convolutional model is examined.

Essentially, the propagating wavelets associated with the top and bottom of the appended layer are convolved with the layers reflection coefficients. This is the dashed blue line. At first, this is confusing because the nonstationary convolution result has a lower frequency content than the Waters' algorithm synthetics. But this illustrates that the multiple interference from the shallow beds has higher frequency propagating wavelets than the ones associated with appended coal layer reflections. In fact, if the synthetic without the appended coal layer is subtracted from the synthetic with the appended coal layer then the blue nonstationary synthetic for the appended coal layer results.

As **d** increases to $\boldsymbol{1000ms}$ (Figure 3.34), the seismic resolution improves because

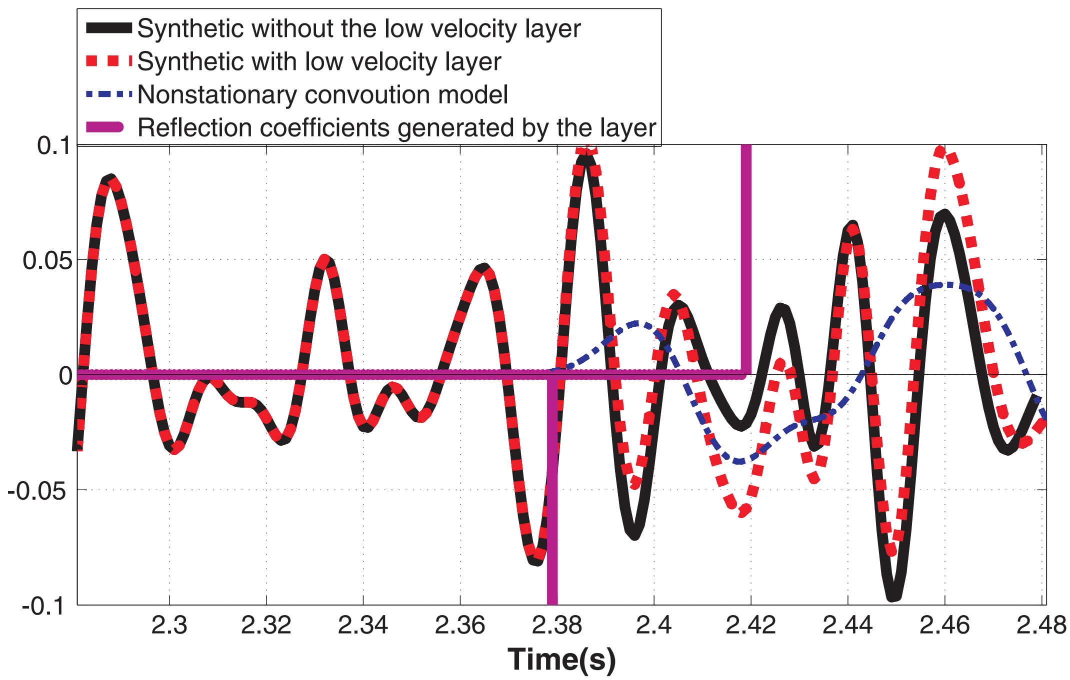

Figure 3.33: Comparison between the multiple synthetics with and without the appended coal layer $\boldsymbol{100ms}$ from the last coal bed. Convolutional modeling of the coal layer using nonstationary propagating wavelets is plotted on the synthetic traces as a blue dashed line.

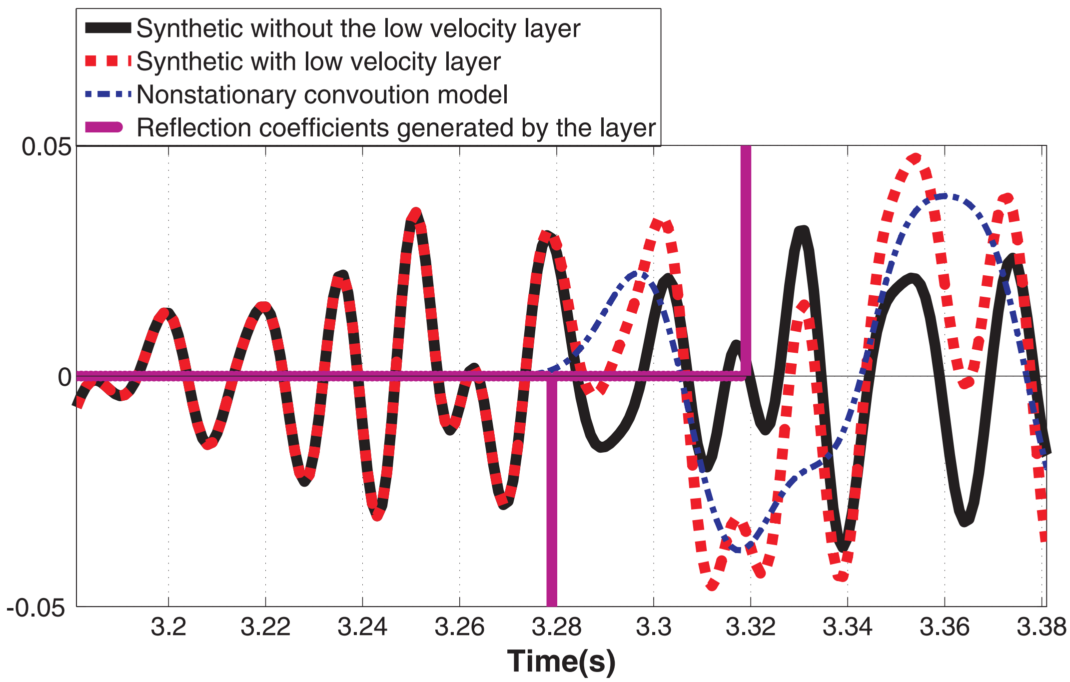

Figure 3.34: Comparison between the multiple synthetics with and without the appended coal layer $\boldsymbol{1000ms}$ from the last coal bed. Convolutional modeling of the coal layer using nonstationary propagating wavelets is plotted on the synthetic traces as a blue dashed line.

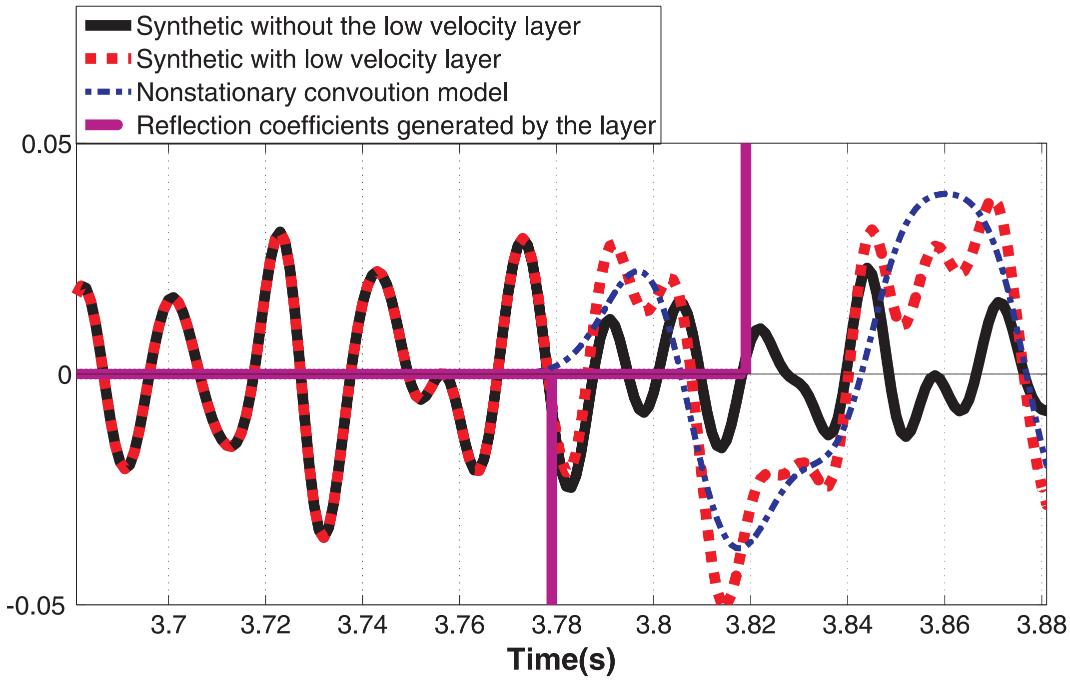

Figure 3.35: Comparison between the multiple synthetics with and without the appended coal layer $\boldsymbol{1500ms}$ from the last coal bed. Convolutional modeling of the coal layer using nonstationary propagating wavelets is plotted on the synthetic traces as a blue dashed line.

there are obvious amplitude differences found between the two synthetic traces. Although the trough and peak in the synthetic considering the coal layer stand out from the synthetic ignoring the coal layer, it is still difficult to locate the top and base of the appended coal layer on the synthetic with the coal layer. When **d** reaches $\boldsymbol{1500ms}$(Figure 3.35), seismic resolution improves greatly so that the middle of the coal layer is uniquely fixed as the zero crossing point between the trough and peak lobes at $\boldsymbol{3.82s}$ and $\boldsymbol{3.86s}$ in the synthetic with the coal layer(red curve) and this looks closer to the nonstationary convolutional model result(blue curve). The

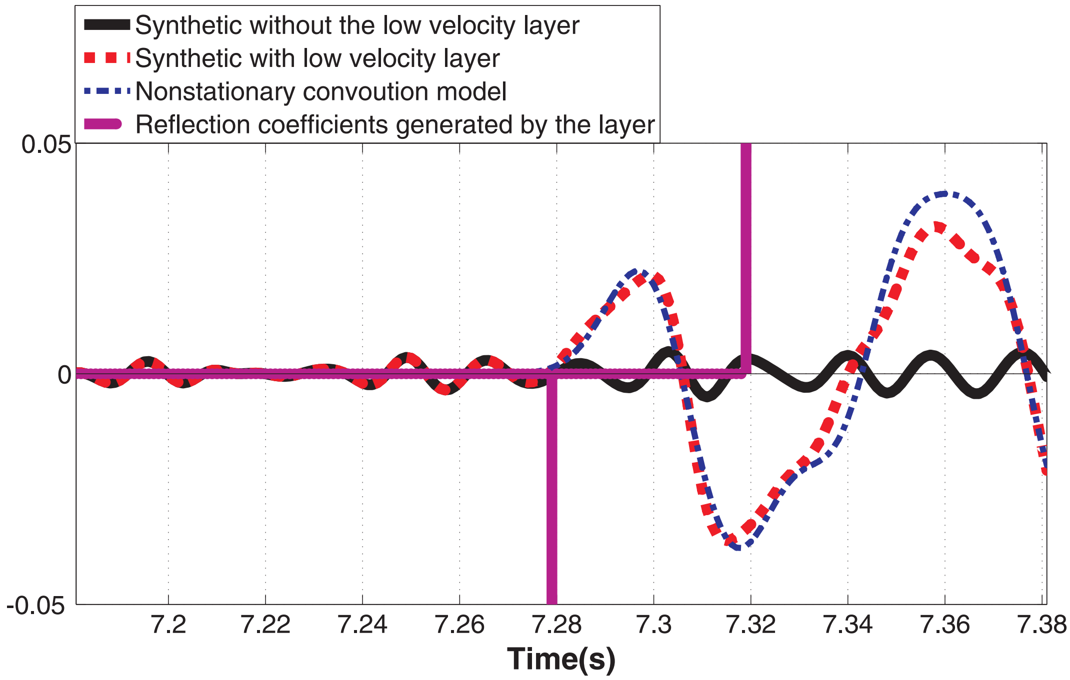

Figure 3.36: Comparison between the multiple synthetics with and without the appended coal layer $\boldsymbol{5000ms}$ from the last coal bed. Convolutional modeling of the coal layer using nonstationary propagating wavelets is plotted on the synthetic traces as a blue dashed line.

measurement of the zero crossing time is $\boldsymbol{3.84s}$ which represents a $\boldsymbol{40ms}$ time delay compared with its primary reflection and that result coincides with the time delay measured in the wavelet dictionary. With this model, the interbed multiples above the coal layer (prior to $\boldsymbol{3.87s}$) have a significantly different frequency content than the seismic response from the append coal layer. It appears that filtering out the high frequencies might make the appended coal layer more visible.

Finally, Figure 3.36 shows the test result when **d** equals to $\boldsymbol{5000ms}$. The resemblance between the synthetic trace with the appended coal layer and the output generated by nonstationary convolutional modeling builds our confidence about the significance of nonstationary convolutional modeling. Once again, the middle of the coal bed is delayed by $\boldsymbol{40ms}$ from the sonic traveltime because of interbed multiples. Likewise, the true reflection is much lower frequency than the remnant multiples of lower amplitude.

One important aspect of Figure 3.36 is the frequency differences between the appended coal layer reflection (low frequency) and the interbed multiple noise frequency (high). The low frequency reflection is actually evident even in Figure 3.33. Thus in order to enhance reflections, bandpass filters based on the spectra of the wavelet dictionary should be applied to suppress the higher frequency multiple energy.

3.5 Estimation of wavelet dictionary

From the previous study, there is definitely an interpretation improvement using nonstationary convolutional modeling in areas where strong interbed multiples dominate. In order to do nonstationary convolution, the wavelet dictionary involving multiple reflections needs to be calculated. At the end of this chapter, methods have been tried to estimate the wavelet dictionary using simple wavelets with minimal coefficients defining the wavelets so that in the future studies these coefficients could possibly be related to specific seismic attributes.

3.5.1 Estimation window

Referring to Figure 3.24 and Figure 3.18, the wavelets in the wavelet dictionary have their energy mainly focus in the first $\boldsymbol{100ms}$, so the estimation length for each wavelet could be limited to the first $\boldsymbol{100ms}$. Figure 3.37 compares the accuracy of the results of nonstationary convolution using varied length wavelet dictionaries. A $\boldsymbol{40Hz}$ Ricker wavelet represents the source wavelet. The $\boldsymbol{600ms}$ wavelet dictionary matches perfectly with the synthetic seismic trace with primary reflections and multiples up to $\boldsymbol{2.5s}$. When the wavelet dictionary is truncated to $\boldsymbol{400ms}$ long, small discrepancies are found at $\boldsymbol{2.41s}$ and this type of discrepancy happens earlier when the wavelet dictionary is truncated to $\boldsymbol{300ms}$. When the wavelet dictionary is truncated to $\boldsymbol{100ms}$, discrepancies start at **2.19**. Except for the truncation length of $\boldsymbol{100ms}$, all discrepancies happen after the time associated with the bottom of coal beds. The hypothesis for these discrepancies is that at the end of coal beds and for several hundred milliseconds below the coal beds, the interbed multiples generated by the shallower coal beds dominate the seismic trace. However, the wavelets associated with the shallower coal beds are truncated and it results the truncation of the interbed multiples from shallower coal beds.

The research focuses on estimating the first $\boldsymbol{100ms}$ of the wavelet dictionary because it is enough to adequately rebuild the reflections in the multiple synthetic at times associated with the main part of the coal beds.

The comparison between the primary-only synthetic with a $\boldsymbol{40Hz}$ Ricker wavelet and the synthetic with multiples (Figure 3.38) shows that only propagating wavelets

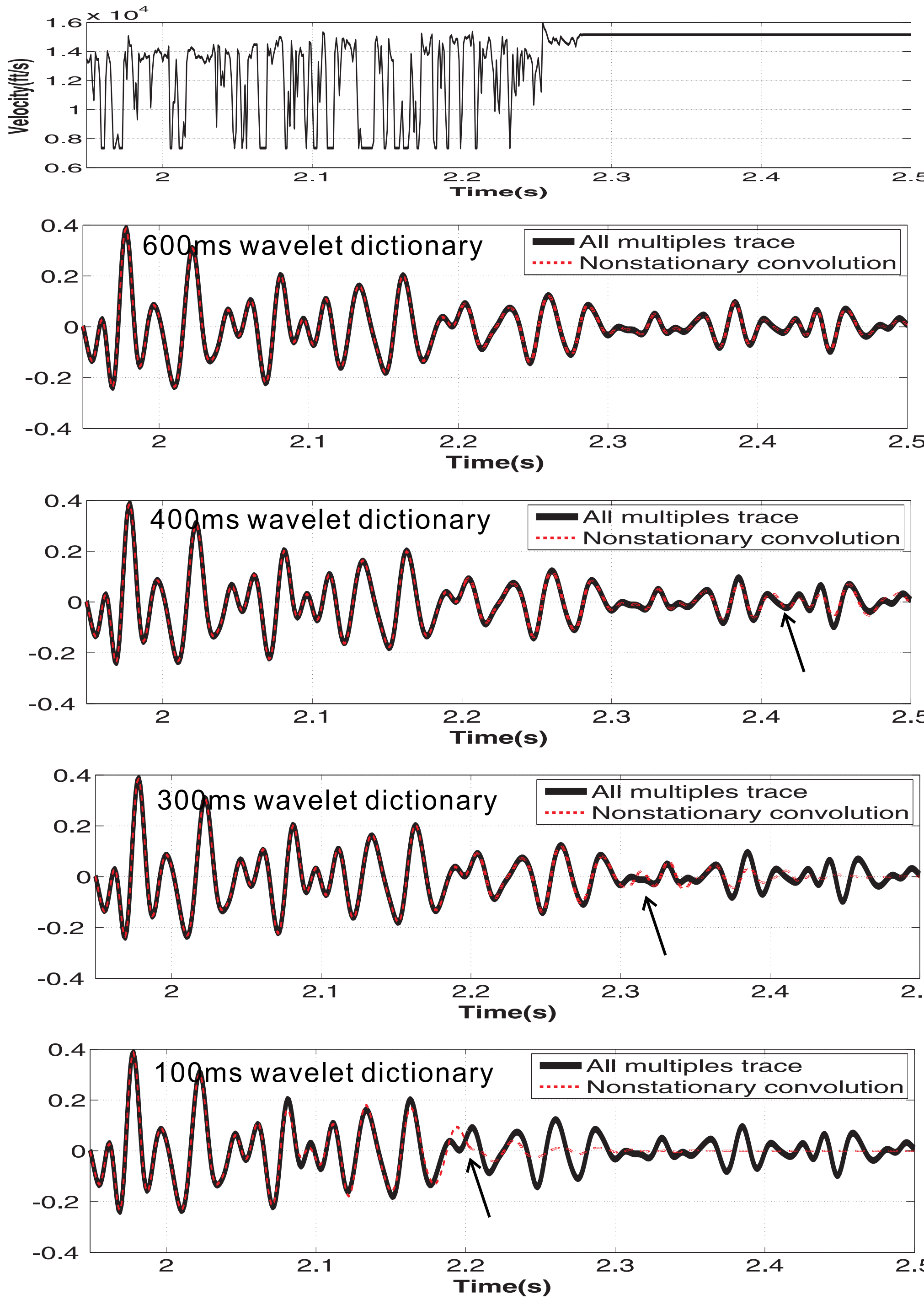

Figure 3.37: Accuracy of nonstationary convolutional modeling when wavelet dictionary is of varied time length.

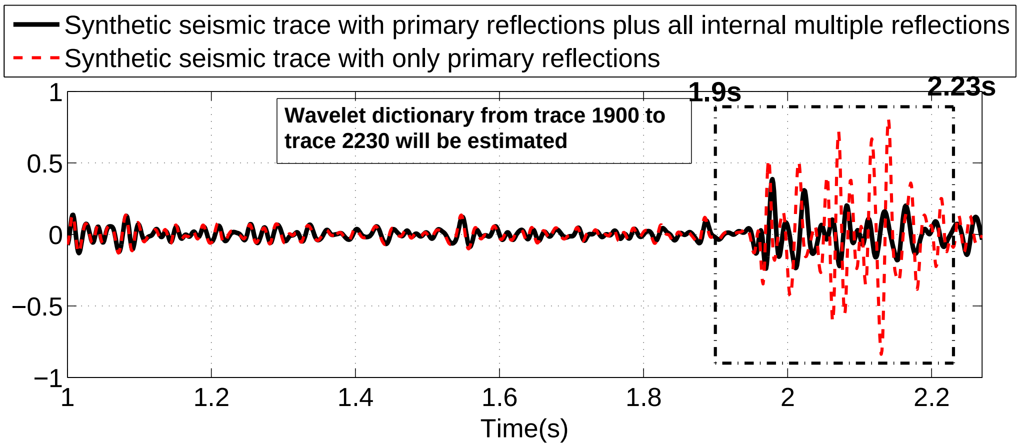

Figure 3.38: Illustration of the range of wavelets that would be estimated in wavelet dictionary. Wavelets whose arrival time is from $\mathbf{1.9}\boldsymbol{s}$ to $\mathbf{2.23}\boldsymbol{s}$ would be estimated.

whose arrival time is between $\mathbf{1.9}\boldsymbol{s}$ to $\mathbf{2.23}\boldsymbol{s}$ need to be estimated because the significant discrepancies between the primary reflections and primary plus multiple reflections occur in this time window.

3.5.2 Fitting wavelet dictionary amplitude spectra using Gaussian function

In Figure 3.24, amplitude spectra are computed for the wavelets truncated at the first $\mathbf{80}\boldsymbol{ms}$ after sonic arrival time. Observing the curve shapes of those spectra, Gaussian functions are used to fit those curves so that each wavelet could be determined by a few Gaussian coefficients if the minimum-delay assumption works for the wavelets. Minimum-delay wavelet is the one with most of its energy concentrated at the beginning (Robinson, 1983), and if the wavelet is minimum-delay its phase spectrum can compute by doing Hilbert-transform on the natural logarithm of its amplitude spectrum.

A nonlinear least-squares regression is used to curve fit the function

$$\boldsymbol{G(f) = A_1 e^{-A_2 f^2}}, \tag{3.4}$$

where $\boldsymbol{A_1}$ and $\boldsymbol{A_2}$ denote the coefficients and $\boldsymbol{f}$ denotes frequency in $\boldsymbol{Hz}$.

The amplitude spectra are fit to the defined Gaussian function, and the results are shown in Figure 3.39 and the coefficients for Gaussian functions are plotted in Figure 3.40. The Gaussian amplitude spectra match the WD wavelets after trace **2170** while the spectra for the shallow depths have slight discrepancies between the wavelets in WD and Gaussian approximations. $\boldsymbol{A_1}$ and $\boldsymbol{A_2}$ may have certain relationships with the velocity log. However, $\boldsymbol{A_1}$ fluctuates around a constant value, approximately **0.8**, and $\boldsymbol{A_2}$ increases with the increasing number of coal layers waves travel through. Further studies are needed to understand more about these coefficients.

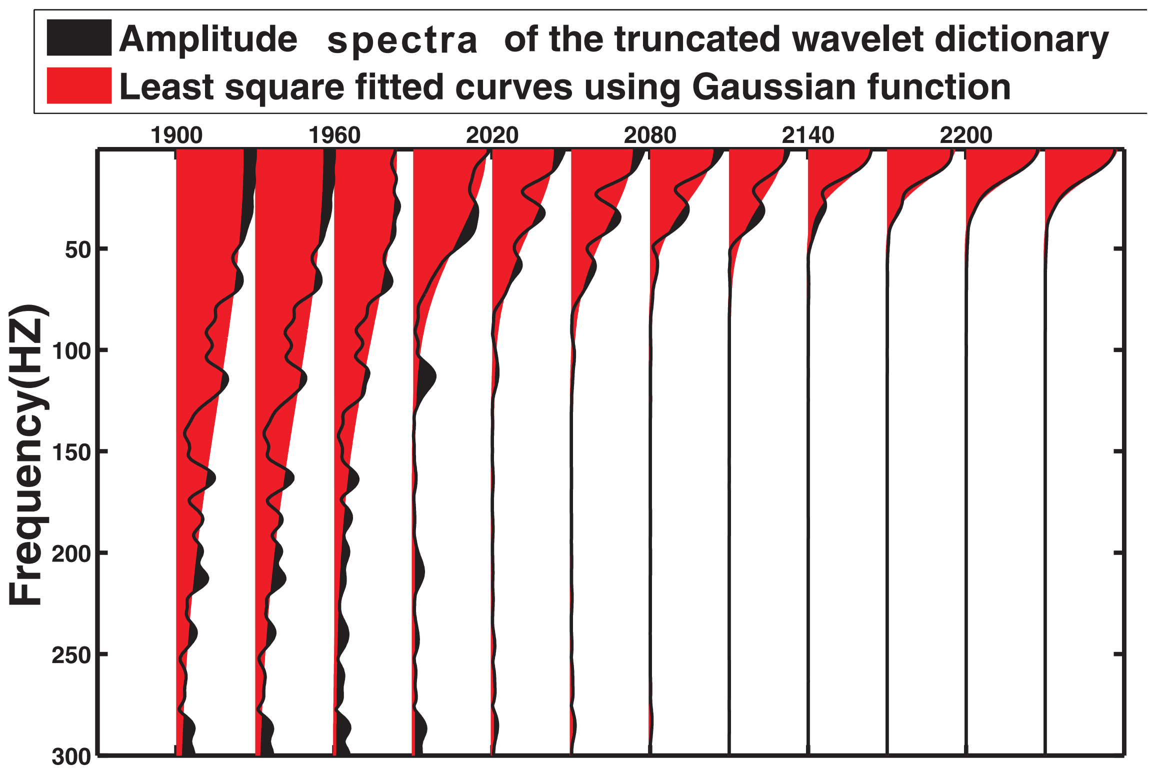

Figure 3.39: Comparison between the amplitude spectra of the truncated wavelet dictionary and the fitted Gaussian curves using nonlinear least squares regression.

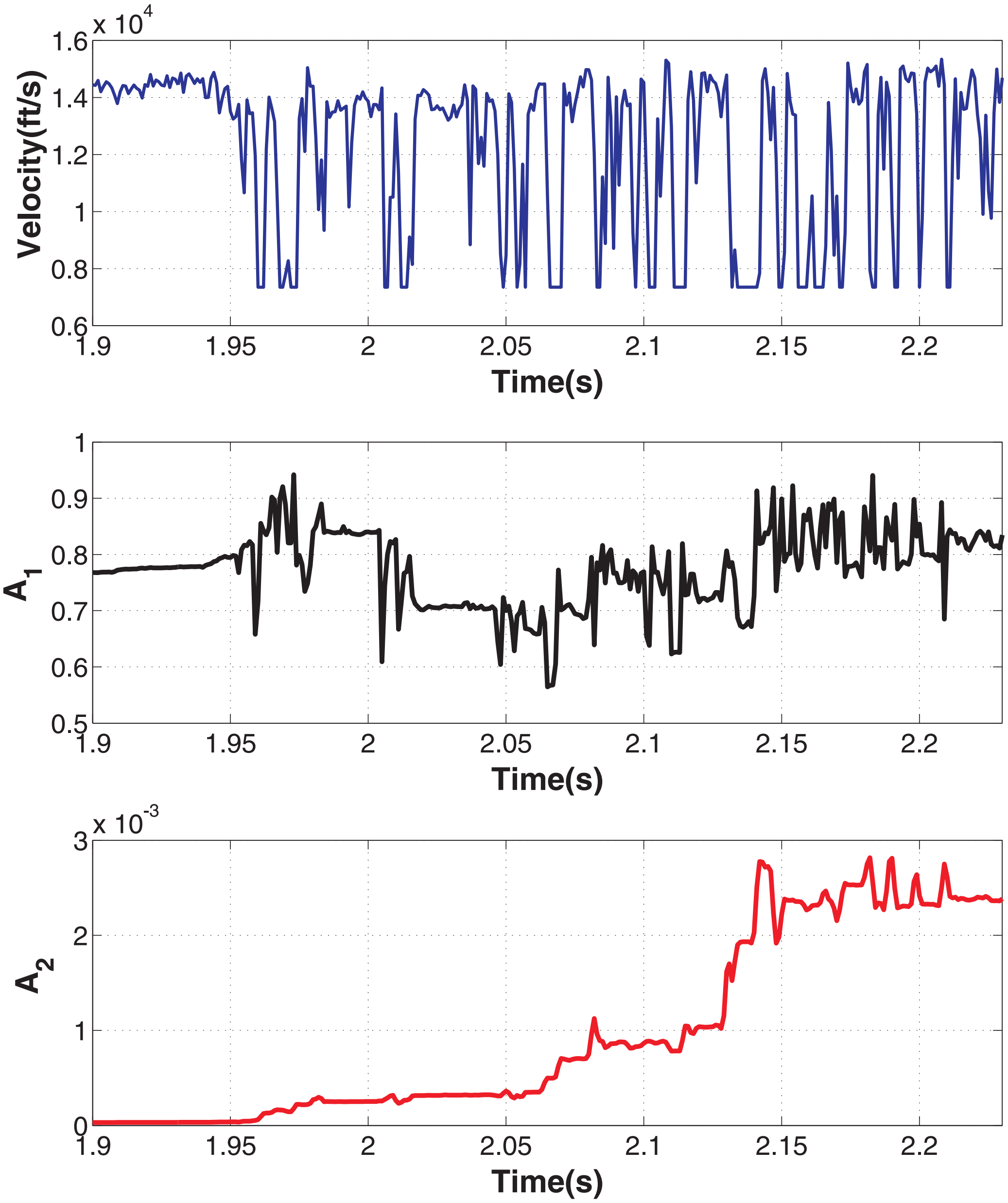

Figure 3.40: Gaussian coefficients extracted by curve fitting amplitude spectra of truncated wavelet dictionary using nonlinear least squares regression.

3.5.3 Reconstruction of wavelet dictionary under minimum delay assumption

Finally, the wavelet dictionary of $\boldsymbol{100ms}$ long is reconstructed using the least-squares amplitude spectra in Figure 3.39 and the comparison between the original wavelet dictionary and the reconstructed wavelet dictionary are shown in Figure 3.41.For traces from **2020** to **2140**, the discrepancies between the reconstructed wavelets and the original wavelets are caused by a dipole phenomenon for the wavelets in original WD and for traces from trace **2140** to the end, the discrepancies are time delays of the original wavelets. However, since the amplitude spectra of traces **2140** to **2260** are fitted perfectly in Figure 3.39, the time delay indicates that the wavelets in wavelet dictionary may be mixed-delay wavelets. This needs additional investigation.

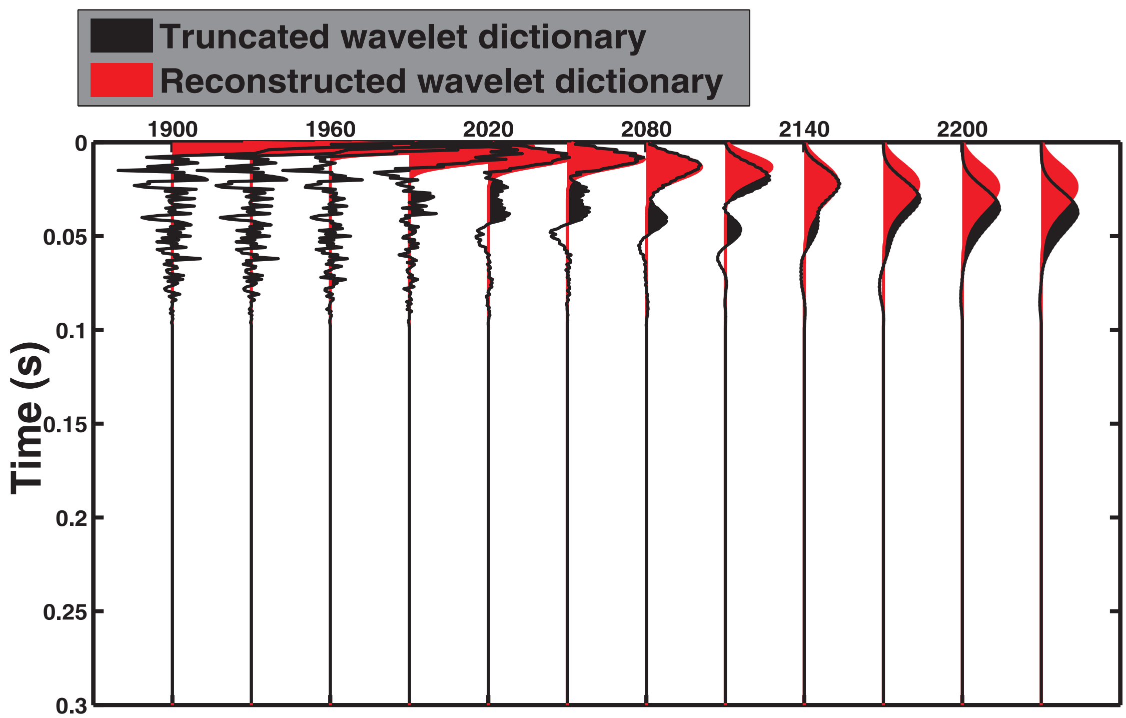

Figure 3.41: Comparison between the **0.1*s*** truncated wavelet dictionary and the reconstructed wavelet dictionary.

3.5.4 Accuracy of doing nonstationary convolution using reconstructed WD

At last, the synthetic seismic trace with all internal multiples is compared with the trace generated by doing nonstationary convolution between the reconstructed wavelet dictionary and the corresponding reflection coefficients. As is shown in Figure 3.42, the discrepancies between the reconstructed wavelet dictionary and the original wavelet dictionary do affect the magnitude of matching at time $\mathbf{2.14}\boldsymbol{s}$ to $\mathbf{2.26}\boldsymbol{s}$. While additional work is needed to improve a mathematically defined WD and its subsequent nonstationary synthetic match, the Gaussian WD is encouraging for interpretation.

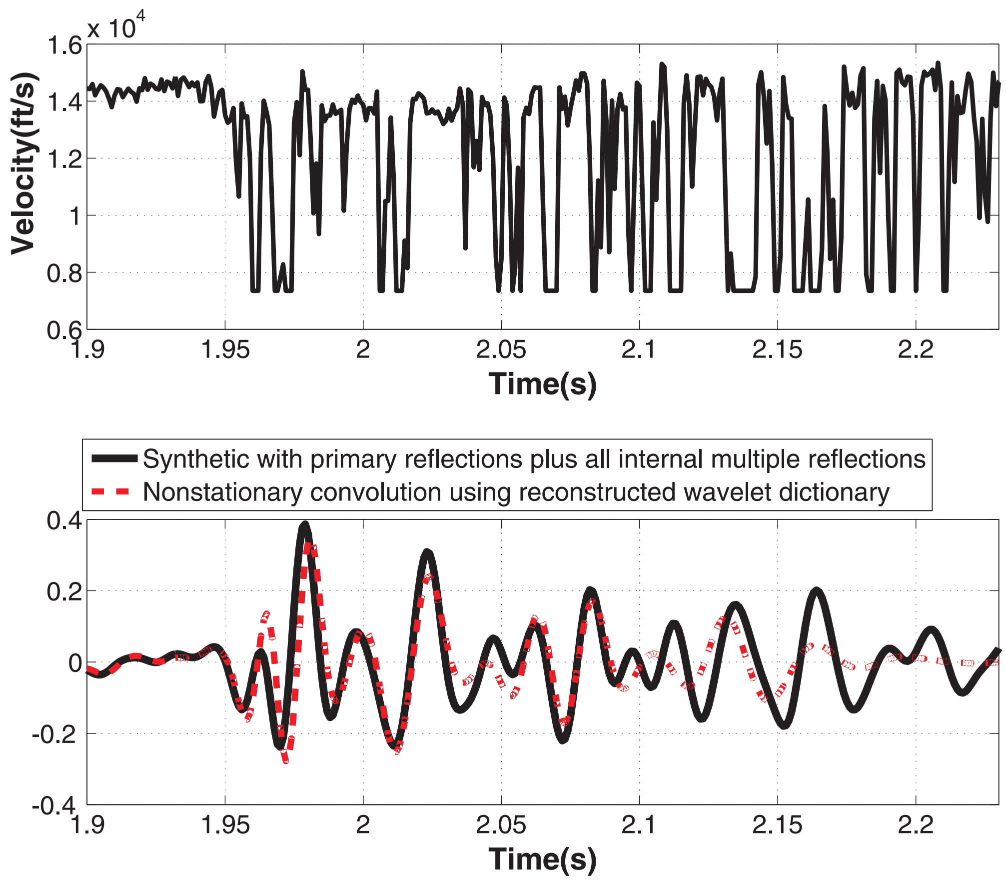

Figure 3.42: Comparison between the synthetic trace with primary reflections plus all internal multiple reflections and the nonstationary convolution result using reconstructed wavelet dictionary.

Chapter 4

Conclusion

The purpose of the thesis is to develop an interpretation method to study interbed multiples and provide information that could be used in seismic processing to remove the effect of interbed multiples as much as possible. In order to do this, nonstationary convolution theory is used. By modifying the convolutional matrix in the nonstationary convolution equation, attenuation effects caused by interbed multiples are added into the nonstationary convolution output. The algorithm of generating such wavelet dictionary has been described.

In order to verify the algorithm generating wavelet dictionary, field data is analyzed and utilized as the source to generate a wavelet dictionary. Different editing procedures have been done on the sonic log in order to reach a satisfying well-tie result. Forcing all coal beds to have the same interval velocity appeared to be a successful editing procedure. The excellent well-tie builds confidence of the algorithm for generating synthetics with all internal multiples. It is found that the near-offset stack matches the synthetic better than the full stack. The wavelet dictionary built from pure propagating wavelets when combined with nonstationary convolution provides a perfect synthetic match to the more conversional method of computing all internal multiple synthetics.

The perfect match proves the correctness of the algorithm for creating a wavelet dictionary. Furthermore, attenuation effects caused by interbed multiples in coal beds are studied using the wavelet dictionary. The frequency band of the wavelets in the wavelet dictionary is narrowed down from the wavelet reflected at the top of coal bed sequence to that at the last coal bed. After the coal beds, the reflection wavelet's amplitude spectrum is similar to a Gaussian function with a half-amplitude occurring at $\boldsymbol{25Hz}$. Time delays caused by interbed multiples are determined by picking the delayed time of the maximum amplitude in each wavelet in wavelet dictionary. The maximum delay time reaches $\boldsymbol{38ms}$.

In order to enhance primary reflections over multiple energy, bandpass filters based on the WD spectra should be applied to field data with nonstationary filtering. The energy loss in the primary reflections is compared with the energy loss in the wavelet dictionary and the result coincides with the conclusions of O'Doherty and Anstey (1971) that interbed multiples tend to preserve seismic reflection energy.

Seismic vertical resolution among and below coal beds has been studied by doing tests computing multiple synthetics with and without the studied coal layer. The seismic vertical resolution is weakened by interbed multiples generated by shallow coal beds and thus reflections after the middle of the coal bed sequence are hard to identify. The rate of time-delay caused by interbed multiples is $\boldsymbol{1ms/1000ft}$

($\boldsymbol{304m}$) for the depth interval from the top of the measured log to the top of coal beds and is $\boldsymbol{25.6ms/1000ft}$ ($\boldsymbol{304m}$) for the depth interval from the top of the coal beds to the bottom of the coal beds.

Finally,a $\boldsymbol{100ms}$ truncated wavelet dictionary is developed by estimating Gaussian functions that match the measured propagating amplitude spectra. The phase spectra are assumed to be minimum phase. More work needs to be done to correct discrepancies between the Gaussian WD and the measure WD synthetics created with nonstationary convolution.

One of the more significant observations during this study might be the possibility of resolving primary reflections from interbed multiples by using a WD to define the broadening of the propagating wavelets. This definition of the propagating wavelet would then be used to enhance by processing the primary energy over the multiple energy. Initial observations indicate that low-pass filtering might be one of the methods to improve the recognition of primary events.

References

Backus, G. E., 1962, Long wave elastic anisotropy produced by horizontal layering: Journal Geophys. Res., **67**, 4427–4440.

Goupillaud, P. L., 1961, An approach to inverse filtering of near-surface layer effects from seismic records: Geophysics, **26**, 754–760.

Liner, C., 2004, Elements of 3-d seismology: Pennwell Pub.

Margrave, 1997, Nonstationary filtering: Review and update: Technical report, Consortium for Research in Elastic Wave Exploration Seismology. (Published).

Margrave, G. F., 1998, Theory of nonstationary linear filtering in the fourier domain with application to time-variant filtering: Geophysics, **63**, 244–259.

Margrave, G. F., M. P. Lamoureux, and D. C. Henley, 2011, Gabor deconvolution: Estimating reflectivity by nonstationary deconvolution of seismic data: Geophysics, **76**, W15–W30.

Mukerji, T., G. Mavko, D. Mujica, and N. Lucet, 1995, Scale-dependent seismic velocity in heterogeneous media: Geophysics, **60**, 1222–1223.

O'Doherty, R. F., and N. A. Anstey, 1971, Reflections on amplitudes: Geophysiccal Prospecting, **19**, 430–458.

Robinson, E. A., 1983, Digital seismic inverse methods: International Human Resources Development Corporation. (Published).

Schoenberger, M., and F. K. Levin, 1974, Apparent attenuation due to intrabed multiples: Geophysics, **39**, 278–291.

Sengbush, R., 1983, Seismic exploration methods: Pexcon International Inc.

Sheriff, R. E., 1991, Encyclopedic dictionary of applied geophysics: Society of Exploration Geophysicists.

Stewart, R. R., P. D. Huddleston, and T. K. Kan, 1984, Seismic versus sonic velocities: A vertical seismic profiling study: Geophysics, **49**, 1153–1168.

Strang, G., 2007, Computational science and engineering: Wellesley-Cambridge Press.

Thomsen, L., 1986, Weak elastic anisotropy: Geophysics, **51**, 1954–1966.

Trorey, A. W., 1962, Theoretical seismograms with frequency and depth dependent absorption: Geophysics, **27**, 766–785.

Waters, K. H., 1981, Reflection seismology: John Wiley and Sons Inc.

Yilmaz, O., 2001, Seismic data analysis: Processing, inversion and interpretation of seismic data: Society of Exploration Geophysicists.

Ziolkowski, A., 1984, Deconvolution: International Human Resources Development Corporation. (Published).